11 Stable Isotopes

Stable isotope geochemistry has become an important discipline within the earth sciences. It is a discipline that is applicable to almost all studies, from those concerning the paleoecology of extinct life forms to those that seek answers about the origin of the earth and solar system.

Kyser (1987c)

In this chapter we will discuss stable isotopes whose abundances in geologic materials vary not as a function of time (because they are not daughter atoms of radionuclides) but because of separation of light from heavy isotopes as a result of various equilibrium and kinetic processes. A large number of stable isotopes occur naturally, but modern stable isotope geochemistry has traditionally been involved with isotopes of a few light elements such as H, C, N, O, and S. Each of these elements has a lighter, more abundant isotope and one or more heavier, less abundant isotopes, the ratios of which vary differentially in natural substances (Table 11.1). The characteristics that render stable isotopes of these elements useful for interpretation of some geochemical and biological processes are as follows (O'Neil, 1986a).

(1) These elements are the main components of most minerals, rocks, and fluids; they also are the basic constituents of most forms of life.
(2) The relative difference in mass between heavy and light isotopes of each of these elements is fairly large (Table 11.1), much more pronounced than in the case of isotopes of heavier elements (e.g., ^{238}U and ^{235}U). The difference ranges from a high of 100% for hydrogen (^{1}H and ^{2}H) to a low of 6.25% for sulfur (^{32}S and ^{34}S). The relative mass difference is an important consideration for *mass-dependent fractionation* of stable isotopes. Hydrogen isotope fractionations, for example, are about ten times larger than those of the other elements of interest.
(3) The occurrence of more than one oxidation state, as with C, N, and S, or of very different types of bonds as in H–O, C–O or Si–O (ranging from ionic to highly covalent) enhances the mass-dependent isotopic fractionation of these elements.
(4) For each of the five elements of interest, the abundance of the least common isotope is sufficiently high (a few tenths of a percent to a few percent) to allow for high precision measurements. Depending on the instrument used, the analytical error of deuterium analysis is up to ten times larger than those of heavier elements because of the low abundance of deuterium (about 160 ppm) in nature.

In contrast, fractionation of isotopes of the elements useful in radiogenic isotope geochemistry (e.g., Sr, Nd, Hf, Os, Pb, etc.) are quite small and can generally be ignored. This is because these elements form dominantly ionic bonds, generally exist in one oxidation state, and are characterized by only small differences in mass between heavy and light isotopes of interest.

Variations of stable isotope ratios in minerals, rocks, and fluids have provided valuable insights into a wide spectrum of geologic issues, ranging in scale from the formation of individual

Introduction to Geochemistry: Principles and Applications, First Edition. Kula C. Misra.

Table 11.1 Abundances of selected stable isotopes and reference standards used for measurement of isotope ratios.

Element	Isotope	Relative abundance (%)	Primary reference standard	Comments
Hydrogen	^{1}H (protium)	99.9844	V–SMOW* (Vienna Standard Mean Ocean Water)	$(D/H)_{SMOW} = 155.76 \times 10^{-6}$
	^{2}H (D)	0.0156		$(D/H)_{SMOW} = 1.050\ (D/H)_{NBS-1}$
Carbon	^{12}C	98.89	PDB (Pee Dee Belemnite)	$(^{13}C/^{12}C)_{PDB} = 1123.75 \times 10^{-5}$
	^{13}C	1.11		
Nitrogen	^{14}N	99.63	N_2 in the atmosphere	$(^{15}N/^{14}N)_{atm} = 361.3 \times 10^{-5}$
	^{15}N	0.37		
Oxygen	^{16}O	99.763	V–SMOW* (Vienna Standard Mean Ocean Water)	$(^{18}O/^{16}O)_{SMOW} = 2005.2 \times 10^{-6}$
	^{17}O	0.0375		$(^{18}O/^{16}O)_{SMOW} = 1.008\ (^{18}O/^{16}O)_{NBS-1}$
	^{18}O	0.1995		
			V–PDB** (Pee Dee Belemnite)	$(^{18}O/^{16}O)_{PDB} = 2067.2 \times 10^{-6}$
Sulfur	^{32}S	95.02	CDT (Canyon Diablo Troilite)	$(^{34}S/^{32}S)_{CDT} = 449.94 \times 10^{-4}$
	^{33}S	0.75		
	^{34}S	4.21		
	^{36}S	0.02		

* Original supplies of SMOW and PDB have been exhausted; V-SMOW and V-PDB are identical to SMOW and PDB, respectively, within limits of analytical errors.
** $\delta^{18}O_{V\text{-}SMOW} = 1.03091\ \delta^{18}O_{PDB} + 30.91$; $\delta^{18}O_{PDB} = 0.97002\ \delta^{18}O_{SMOW} - 29.98$.
Source of data: compilations by Kyser (1987a, p. 2) and O'Neil (1986b).

minerals to the evolution of the Earth and its biosphere through time. Some notable applications of these isotopes include: geothermometry; recognition and quantification of crustal assimilation by magmas and mixing of hydrothermal fluids; inferences about the sources of sulfide, sulfate, carbonate, reduced carbon, and metals in rocks and ore deposits; estimation of water : rock ratios in water–mineral reactions; and tracing the evolution of the atmosphere–biosphere system. In this chapter we will focus on a few such applications of oxygen–hydrogen and sulfur isotopes. More detailed treatments of stable isotope geochemistry can be found in Faure (1986, 2001), Valley *et al.* (1986), Kyser (1987c), Criss (1999), Hoefs (2004), and Anbar and Rouxel (2007).

Studies of stable isotope geochemistry, however, have not been limited to the few traditional elements mentioned above (O, H, S, C, and N). With the advent of advanced analytical instruments such as multicollector, inductively coupled plasma mass spectrometers (MC–ICP–MS), capable of attaining precisions of 0.05 to 0.2 per mil (‰) for many isotope systems, large portions of the Periodic Table are now accessible to stable isotope studies. The isotopic geochemistry of a number of nontraditional stable isotopes of elements, such as Li, Mg, Cl, Ca, Cr, Fe, Cu, Zn, Se, and Mo, is being seriously investigated, and has been reviewed recently in Johnson *et al.* (2004a). Some innovative applications of nontraditional isotopes include reconstruction of the paleochemistry of the oceans (Ca, Fe, Mo), fingerprinting the source of contaminants in groundwater (Cr, Cu, Zn, Cd), and the monitoring of metal transfer processes in the human body (Fe, Ca). As the brief discussion of Fe isotopes included in this chapter would illustrate, nontraditional stable isotopes are governed by the same general principles as the traditional stable isotopes.

11.1 Isotopic fractionation

The partitioning of isotopes of an element between two coexisting substances resulting in different isotopic ratios in the two substances is called *isotopic fractionation*. The isotopes of an element have nearly identical electronic structure and, therefore, very similar chemical properties, but the mass difference causes the stable isotopes to fractionate during certain reactions. Biological and most geological processes produce such mass-dependent fractionation.

11.1.1 Causes of isotopic fractionation

The energy of a molecule can be described in terms of the interactions among the electrons as well as different kinds of motions of atoms in a molecule: vibrational (the stretching and compression of the chemical bonds between the atoms), rotational, and translational (linear motion). Isotopic fractionation arises largely because such motions are

associated with energies that are mass dependent. By far the largest contribution comes from vibrational motion, the only mode of motion available to atoms in a solid substance. For a molecule, $E_{\text{vibrational}} = 1/2\ h\upsilon$, where E = virational energy, ν = vibrational frequency, which is inversely proportional to the square root of its mass, and h = Planck's constant. In the case of hydrogen and deuterium, differences in the rotational component are also important. Isotopic fractionation between two chemical species results in redistribution of the isotopes of interest to minimize the energy of the system. So, when a heavier isotope of an element replaces a lighter isotope, the vibrational energy of the molecule is decreased and the molecule tends to be more stable compared with a molecule containing the lighter isotope. As a general rule, between coexisting molecules the heavier isotope is preferentially partitioned into the one in which it can form the stronger bond, that is, the bond associated with lower vibrational frequency. For example, in a liquid–vapor system, such as H_2O (liquid)–H_2O (vapor), the liquid phase with stronger bonds is enriched in the heavier isotopes (^{18}O and ^{2}H), whereas the vapor phase with weaker bonds preferentially concentrates the lighter isotopes (^{16}O and ^{1}H).

Another reason for mass-dependent fractionation of isotopes is the kinetic energies of molecules. The kinetic energy of a molecule is a function of its mass ($E_{\text{kinetic}} = 1/2\, m\upsilon^2$, where m = mass and υ = velocity), and is the same for all ideal gases at a given temperature. Differences in the velocities of isotope molecules lead to isotopic fractionations in a variety of ways. Isotopically light molecules, such as $^{12}C^{16}O$, can preferentially diffuse out of a system and leave the residual reservoir enriched in the heavy isotope $^{12}C^{18}O$. In the case of evaporation of water, the greater average translational velocity of the lighter $^{1}H_2{}^{16}O$ molecules allows them to break through the liquid surface preferentially, resulting in an isotopic fractionation between vapor and liquid (O'Neil, 1986a).

11.1.2 Mechanisms of isotopic fractionation

The main mechanisms for fractionation of stable isotopes are (Faure, 1986; Hoefs, 2004):

(1) isotopic exchange reactions, which involve the redistribution of isotopes of an element among different molecules containing that element, without any change in the chemical make-up of the reactants or products;
(2) unidirectional reactions, such as bacterially mediated reduction of sulfate species to sulfide species, in which reaction rates depend on isotopic compositions of the reactants and products; and
(3) physical processes such as evaporation and condensation, melting and crystallization, adsorption and desorption, and diffusion of ions or molecules due to concentration or temperature gradients, in which mass differences come into play.

11.1.3 Fractionation factor

Irrespective of mechanism, the degree of isotopic fractionation between two coexisting phases A and B in isotopic equilibrium is expressed by a ratio called the *fractionation factor,* α_{A-B}, which is defined as:

$$\boxed{\alpha_{A-B} = \frac{R_A}{R_B}} \tag{11.1}$$

where R is an atomic ratio and by convention is always written as the ratio of heavy (less abundant) isotope to the light (more abundant) isotope (such as D/H, $^{13}C/^{12}C$, $^{15}N/^{14}N$, $^{18}O/^{16}O$, or $^{34}S/^{32}S$) in the phase indicated by the subscript. For example, the fractionation factor describing the fractionation of the carbon isotopes ^{13}C and ^{12}C between calcite and CO_2 is defined as:

$$\alpha_{\text{calcite}-CO_2} = \frac{\left(^{13}C/^{12}C\right)_{\text{calcite}}}{\left(^{13}C/^{12}C\right)_{CO_2}} \tag{11.2}$$

which has an empirically determined value of 1.0098.

Isotopic fractionation factor is analogous to the distribution coefficient and is the most important quantity used in evaluating stable isotope variations observed in nature. Factors influencing the sign and magnitude of fractionation factors are (O'Neil, 1986a): (i) temperature; (ii) chemical composition; (iii) crystal structure and chemical bonds; and (iv) pressure. The variation of fractionation factors as a function of temperature can be quite pronounced in some systems and is the basis of stable isotope geothermometry (discussed later). In general, bonds to ions with low atomic mass and high ionic potential are associated with high vibrational frequencies, and such ions tend to incorporate the heavy isotope preferentially in order to lower the free energy of the system. Thus, molecules containing the heavier isotope (e.g., ^{13}C–H, ^{34}S–O) have higher dissociation energies and are more stable than those containing the lighter isotope (e.g., ^{12}C–H, ^{32}S–O). In natural equilibrium assemblages, quartz in which the oxygen is bonded to the small, highly charged Si^{4+} ion is considerably enriched in ^{18}O, whereas magnetite in which the oxygen is bonded to the relatively large and divalent Fe^{2+} ion is ^{18}O-deficient. Similarly, carbonate minerals are ^{18}O-rich because the oxygen in these minerals is bonded to the small, highly charged C^{4+} ion. Effects of crystal structure on the fractionation factor are commonly minor in importance compared to those arising from chemical bonding, but can be large in some cases. For example, the ^{18}O fractionation between aragonite and calcite is only about 1.0‰ at 25°C, but that between H_2O and D_2O, the latter with a more ordered structure, is more than 15‰ at 25°C. The effect of pressure on fractionation in solid phases is negligible, no more than 0.1‰ over

20 kbar, because the change in molar volumes of solids on isotopic substitution is very small, typically hundreds to tenths of a percent; the effect may, however, be significant in mineral–fluid systems.

Fractionation factors are obtained in three ways (O'Neil, 1986a): (i) semi-empirical calculations using spectroscopic data and the methods of statistical mechanics; (ii) laboratory calibration studies; and (c) measurements of natural samples whose formation conditions are well known or highly constrained. Experimentally or empirically determined fractionation factors for a large number of systems are listed in O'Neil (1986a), Kyser (1987a), and Campbell and Larsen (1998).

11.1.4 The delta (δ) notation

It is easier and more precise to measure the difference in absolute isotope ratios between two substances than the value of R in each substance. As such stable isotope ratios are normally reported as delta (δ) values in units of parts per thousand or per mil (‰) relative to appropriate reference standards. For a sample, δX_{sample} is defined as:

$$\boxed{\delta X_{sample}(\text{per mil}) = \frac{\left(R_{sample} - R_{std}\right)}{R_{std}} \times 10^3} \tag{11.3}$$

where R_{sample} is the atomic ratio of the heavy to the light isotope in the sample, R_{std} is the corresponding ratio in the standard, and δX stands for δD, δ^{18}O, δ^{34}S, δ^{13}C, or δ^{15}N. The oxygen isotope ratio of a carbonate sample, for example, is reported as

$$\delta^{18}O_{sample}(\text{per mil}) = \frac{(^{18}O/^{16}O)_{carbonate} - (^{18}O/^{16}O)_{std}}{(^{18}O/^{16}O)_{std}} \times 10^3 \tag{11.4}$$

Carbon dioxide is the most suitable gas for analysis of oxygen isotope ratios, which are measured directly with an isotope ratio mass spectrometer. The isotope composition of oxygen in water is determined by analysis of CO_2 that was equilibrated isotopically with the water sample at a known temperature. The isotopic composition of hydrogen in water is measured by analysis of H_2 gas that was prepared by reacting the water sample with metallic uranium at about 750°C. The isotopic composition of oxygen in a carbonate sample is determined from CO_2 gas obtained by reacting the sample with 100% phosphoric acid, commonly at 25°C. In an actual mass spectrometer run, the isotope ratio of the unknown sample gas is compared repeatedly with the isotope ratio of a standard gas derived from the appropriate reference standard by rapidly switching back and forth between sample and standard by means of a magnetically operated valve system. This ensures that the two gases are measured under identical spectrometer conditions. The precision of δ^{18}O values is of the order of ±0.2% or better, including instrumental, analytical, and sampling errors; the corresponding precision of δD values is ±1%.

The convention of expressing δX in per mil (instead of percent) is to avoid dealing with very small numbers. It follows from the definition of δX that for a standard $\delta X = 0$. A positive value of δ means enrichment of the heavier isotope in the sample relative to the standard, a negative value indicates relative depletion of the heavier isotope in the sample. For example, a sample with $\delta^{18}O = -10‰$ is depleted in $^{18}O/^{16}O$ ratio by 10.0‰ (or 1%) relative to the standard. Typical ranges of oxygen, sulfur, and carbon isotope ratios in natural geologic systems are summarized in Fig. 11.1.

Isotope laboratories use various working standards for the measurement of δ values, but to facilitate interlaboratory comparisons, the δ values are scaled to internationally accepted standards (Table 11.1). Troilite (FeS) from the Canyon Diablo iron meteorite is the standard used for reporting δ^{34}S values. The standard commonly used for reporting δ^{18}O and δ D values is SMOW (Standard Mean Ocean Water), which was defined by Craig (1961) in terms of a National Bureau of Standards (USA) reference water, NBS-1, as follows:

$$\begin{aligned} (^{18}O/^{16}O)_{SMOW} &= 1.008\ (^{18}O/^{16}O)_{NBS\text{-}1} \\ (D/H)_{SMOW} &= 1.050\ (D/H)_{NBS\text{-}1} \end{aligned} \tag{11.5}$$

The universally employed reference standard for reporting δ^{13}C values is the Chicago PDB standard (Belemnite from the Cretaceous Peedee Formation, South Carolina), which was the laboratory working standard used at the University of Chicago during the time that the oxygen isotope paleotemperature scale was being developed. The original SMOW and PDB standards have been exhausted. V-SMOW and V-PDB, whose scales are identical to those of SMOW and PDB within the limits of analytical uncertainty, refer to standards available from the International Atomic Energy Commission (IAEA) in Vienna. A commonly employed silicate standard at present is NBS-28 quartz, which has $\delta^{18}O = +9.60‰$ on the SMOW scale. A relatively new working standard for carbon isotopes is the carbonate reference standard NBS-19, which is scaled as:

$$\delta^{13}C_{NBS\text{-}19/PDB} = 1.95‰ \tag{11.6}$$

11.1.5 Calculation of the fractionation factor from δ values

Isotopic fractionation factors can be approximated in terms of δ values. For two species, A (reactant) and B (product), coexisting in isotopic equilibrium, the relationship is (see Box 11.1 for derivation):

$$\boxed{1000 \ln \alpha_{A-B} \approx \delta_A - \delta_B = \Delta_{A-B}} \tag{11.7}$$

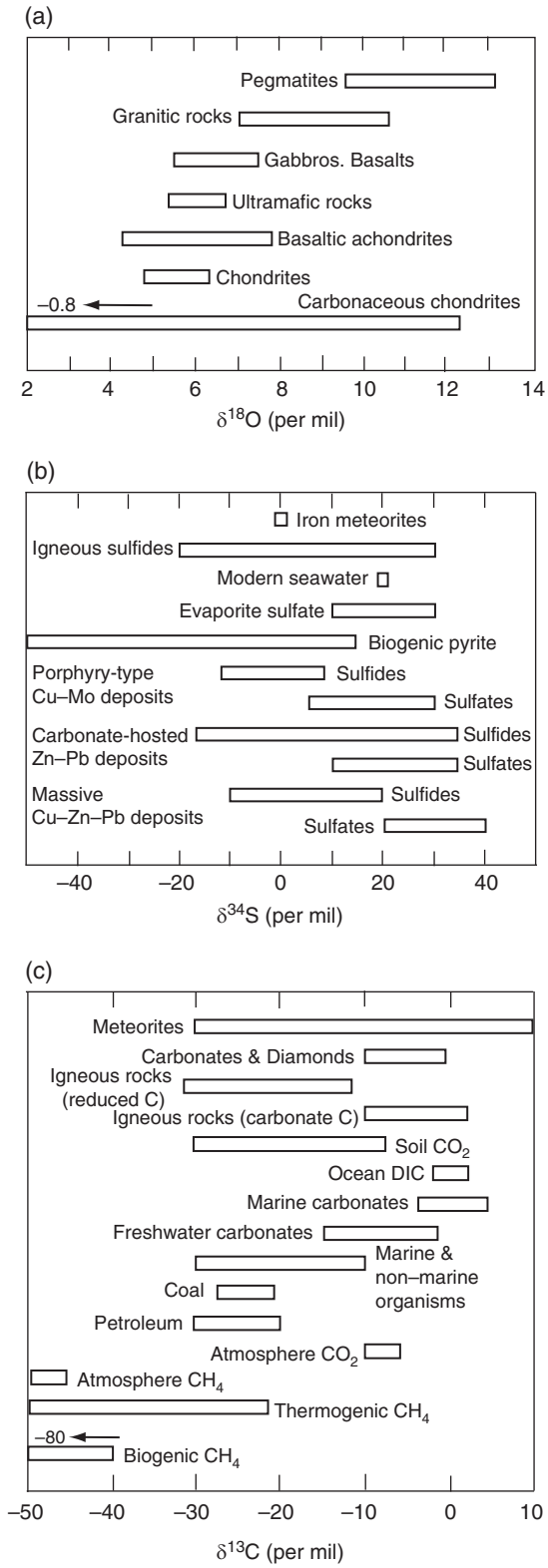

Fig. 11.1 Typical ranges of stable isotope ratios in geologic systems: (a) Oxygen; (b) Sulfur; (c) Carbon. (Sources of data: compilations by Faure (1986), Hoefs (1997), and Misra (2000).)

Box 11.1 Relationship between isotopic fraction factor and δ values for two species A and B coexisting in equilibrium (A⇔B)

From **equation** (11.3),

$$\delta_A = \left(\frac{R_A}{R_{std}} - 1\right) \times 10^3; \quad \delta_B = \left(\frac{R_B}{R_{std}} - 1\right) \times 10^3 \tag{11.8}$$

which can be rearranged to obtain expressions for R_A, R_B, and R_A/R_B in terms of δ_A and δ_B:

$$R_A = \left(\frac{\delta_A + 1000}{1000}\right) R_{std}; \quad R_B = \left(\frac{\delta_B + 1000}{1000}\right) R_{std} \tag{11.9}$$

$$\boxed{\alpha_{A-B} = \frac{R_A}{R_B} = \frac{\delta_A + 1000}{\delta_B + 1000}} \tag{11.10}$$

From equation (11.1),

$$\alpha_{A-B} - 1 = \frac{R_A}{R_B} - 1 = \frac{R_A - R_B}{R_B} \tag{11.11}$$

Substituting for R_A and R_B in equation (11.11),

$$\alpha_{A-B} - 1 = \frac{\delta_A - \delta_B}{\delta_B + 1000} \tag{11.12}$$

Because δ_B is very small compared to 1000, we make the approximation that $\delta_B + 1000 \approx 1000$, and simplify equation (11.12) to:

$$1000\ (\alpha_{A-B} - 1) \approx \delta_A - \delta_B \tag{11.13}$$

Values of α for the light stable isotope pairs (except for the D–H pair) are very close to unity and typically vary in the third decimal place. Most values, therefore, are of the form 1.00X, where X is rarely greater than 4, so that 1000 ln(1.00X) ≈ X. For example, for X = 4 (i.e., α = 1.004), 1000 ln(1.004) = 1000 (0.00399) ≈ 4. This is a useful relationship because experimental studies have shown that 1000 ln α is a smooth, and in some cases a linear, function of temperature for many minral–mineral and mineral–fluid pairs (see section 11.3).

Also, for small values of X, 1000 (1.00X − 1) ≈ 1000 ln(1.00X). Using these approximations,

$$1000 \ln \alpha_{A-B} = 1000\ (\alpha_{A-B} - 1) \tag{11.14}$$

Substituting in equation (11.13),

$$\boxed{1000 \ln \alpha_{A-B} \approx \delta_A - \delta_B = \Delta_{A-B}} \tag{11.7}$$

The isotopic fractionation factor between any two species A and B can also be calculated from either of the following relationships (which can easily be deduced from first principles):

$$\boxed{\alpha_{A-B} = \frac{\alpha_{A-C}}{\alpha_{B-C}}} \tag{11.15}$$

$$\boxed{\Delta_{A-B} = \Delta_{A-C} - \Delta_{B-C}} \tag{11.16}$$

where C denotes a third coexisting species.

where Δ_{A-B} represents the isotopic fractionation between A and B. Fractionation factors obtained by merely subtracting δ values will be in excellent agreement with 1000 ln α, within limits of analytical error, for values of both Δ and δ_i up to about ±10‰ (O'Neil, 1986b, p. 563). For per mil fractionations or δ_i values significantly greater than |10|, as often is the case, for example, in the hydrogen system, calculations should use equations (11.10) or (11.12). Experimentally determined fractionation factors between mineral pairs or mineral–fluid pairs yield smooth curves in 1000 ln α versus $1/T^2$ plots (T in Kelvin), generally above 150°C.

Example 11–1: Calculation of isotopic fractionation factor from δ values

Given that δ values of liquid water (lw) and water vapor (wv) in equilibrium at 10°C are: $\delta^{18}O_{lw}=-0.80$‰, and $\delta^{18}O_{wv}=-10.79$‰, what are the values of Δ_{lw-wv} and the fractionation factor α_{lw-wv} at 10°C?

Using equation (11.7),

$$\Delta_{lw-wv}=\delta_{lw}-\delta_{wv}=-0.80-(-10.79)=+9.99‰$$

$$\ln \alpha_{lw-wv}=(\delta_{lw}-\delta_{wv})/1000=9.99/1000=0.00999$$

$$\alpha_{lw-wv}=e^{0.00999}=1.01004$$

Note that using equation (11.12), we get

$$\alpha_{lw-wv}=\frac{\delta_{lw}-\delta_{wv}}{\delta_{wv}+1000}+1=\frac{9.99}{-10.79+1000}+1$$
$$=0.0101+1=1.0101$$

which is almost identical to the value of α_{lw-wv} calculated above.

11.2 Types of isotopic fractionation

Effects of isotopic fractionation are generally evaluated as: (i) equilibrium isotopic effects, produced by equilibrium isotope exchange reactions, which are independent of the pathways or mechanisms involved in the achievement of equilibrium; and (ii) kinetic isotopic effects, produced by unidirectional processes or unequilibrated chemical reactions (e.g., evaporation, diffusion, bacteria-mediated generation of methane from organic matter), which depend on reaction mechanisms and possible intermediate products.

11.2.1 Equilibrium isotope effects

If CO_2 containing only ^{16}O is mixed with water containing only ^{18}O (although such molecules with only one isotope of oxygen actually do not exist in nature), the two substances will exchange ^{16}O and ^{18}O until the system achieves equilibrium. For ease of mathematical manipulations, isotope exchange reactions are usually written in such a way that only one atom of the isotope is exchanged. For example, the oxygen isotope exchange between $CO_{2(g)}$ and $H_2O_{(l)}$ may be represented as

$$\frac{1}{2}C^{16}O_{2(g)}+H_2{}^{18}O_{(l)}=\frac{1}{2}C^{18}O_{2(g)}+H_2{}^{16}O_{(l)} \qquad (11.17)$$

Isotope exchange equilibrium may be viewed as a special case of general chemical equilibrium in which the isotopes of a single element are exchanged between two different substances, but without any net reaction. The equilibrium constant for this exchange reaction, $K_{CO_2-H_2O}$, is written in terms of concentrations as

$$K_{CO_2-H_2O}=\frac{(C^{18}O_2)^{\frac{1}{2}}(H_2{}^{16}O)}{(C^{16}O_2)^{\frac{1}{2}}(H_2{}^{18}O)}=\frac{(^{18}O/{}^{16}O)_{CO_2}}{(^{18}O/{}^{16}O)_{H_2O}} \qquad (11.18)$$

and it can be calculated using methods of statistical mechanics. Concentrations are used rather than activities or fugacities because ratios of activity or fugacity coefficients for isotopically substituted molecules are equal to unity (O'Neil, 1986a).

If the isotopes are randomly distributed over all possible crystallographic sites in the species involved in the exchange reaction, the fractionation factor (α) is related to the equilibrium constant (K) of the reaction by the relation

$$\alpha_{CO_2-H_2O}=K^{1/n}_{CO_2-H_2O} \qquad (11.19)$$

where n is the number of atoms exchanged. For the reaction under consideration, $n=1$, and the equilibrium constant is identical to the fractionation factor:

$$K_{CO_2-H_2O}=\frac{(^{18}O/{}^{16}O)_{CO_2}}{(^{18}O/{}^{16}O)_{H_2O}}=\frac{R_{CO_2}}{R_{H_2O}}=\alpha_{CO_2-H_2O} \qquad (11.20)$$

The experimentally determined value of $\alpha_{CO_2-H_2O}$ at 25°C (298.15 K) and 1 bar is 1.0412 (Kyser, 1987a), which means that this exchange reaction at equilibrium should result in CO_2 being enriched in ^{18}O by 41‰ relative to H_2O (and H_2O being depleted in ^{18}O by 41‰ relative to CO_2).

The standard-state (298.15 K, 1 bar) Gibbs free energy change for the reaction is a small quantity:

$$\Delta G^1_{r,298}=-RT\ \ln K_{CO_2-H_2O}$$
$$=-(8.314\text{ J mol}^{-1}\text{K}^{-1})\ (298\text{ K})\ (\ln 1.0412)$$
$$=-100.03\text{ J mol}^{-1}$$

In fact, the Gibbs free energy changes for typical isotope exchange reactions in nature are in the order of –100 J mol^{-1} or less, not large enough to initiate chemical reactions. That is why it is not necessary to consider isotopic compositions of the species involved in chemical equilibria. On the other hand, conditions that can break and reform Al–O and S–O bonds to allow equilibrium distribution of ^{18}O among the minerals should be sufficient to establish chemical equilibrium in the system. Thus, oxygen isotope equilibrium among minerals in a rock is strong evidence that the minerals are also in chemical (mineralogical) equilibrium (O'Neil, 1986a).

11.2.2 *Kinetic isotope effects*

Biochemical reactions such as bacterially mediated reduction of sulfate (SO_4^{2-}) to H_2S or generation of methane (CH_4) from organic matter are unidirectional because the rate of backward reaction is much slower than that of the forward reaction, and the reaction does not attain equilibrium. Some chemical reactions such as evaporation, diffusion, and dissociation are also unidirectional. The instantaneous isotopic fractionation accompanying such a unidirectional reaction can be considered in terms of rate constants for the component reactions.

In principle, the exchange of sulfur isotopes ^{32}S and ^{34}S between sulfate (SO_4^{2-}) and its reduced product H_2S can be represented by the exchange reaction

$$^{32}SO_4^{2-} + H_2{}^{34}S = {}^{34}SO_4^{2-} + H_2{}^{32}S \tag{11.21}$$

The calculated theoretical value of the equilibrium constant for this reaction, $K_{SO_4^{2-}-H_2S}$, defined as

$$K_{SO_4^{2-}-H_2S} = \frac{(^{34}SO_4^{2-})\,(H_2{}^{32}S)}{(^{32}SO_4^{2-})\,(H_2{}^{34}S)} = \frac{(^{34}S/^{32}S)_{SO_4^{2-}}}{(^{34}S/^{32}S)_{H_2S}} = \alpha_{SO_4^{2-}-H_2S} \tag{11.22}$$

is 1.075 at 25°C (Tudge and Thode, 1950). Thus, if this exchange takes place, although no mechanism is yet known, it should lead to the enrichment of sulfate in ^{34}S by amounts up to 75‰ relative to H_2S (or the enrichment of H_2S in ^{32}S by amounts up to 75‰ relative to sulfate).

In reality, bacterially mediated reduction of sulfate to H_2S involves two competing isotopic reactions with different mass-dependent rate constants:

$$^{32}SO_4^{2-} \xrightarrow{k_1} H_2{}^{32}S \quad \text{and} \quad {}^{34}SO_4^{2-} \xrightarrow{k_2} H_2{}^{34}S \tag{11.23}$$

For this process, the ratio of rate constants for the two forward reactions, k_1/k_2, is the *kinetic isotopic effect* that measures the extent of isotopic fractionation; i.e., $\alpha_{SO_4^{2-}-H_2S} = k_1/k_2$. The isotopic fractionation in this case occurs because one of the isotopes reacts more rapidly than the other. In general, molecules containing the lighter isotope (e.g., $^{32}SO_4^{2-}$) have the faster reaction rate compared to molecules containing the heavier isotope (e.g., $^{34}SO_4^{2-}$) because of smaller bonding energy, so that the product (H_2S) tends to be enriched in the lighter isotope (^{32}S) and depleted in the heavier isotope (^{34}S) relative to the parent SO_4^{2-} (see section 11.6).

The magnitude of equilibrium fractionation factor between two species is independent of pathway; it depends only on temperature (the effect of pressure is negligible at pressures less than about 10 kbar). The kinetic isotope effect, on the other hand, depends on the reaction pathway. Other factors that influence the magnitude of kinetic isotope effect are those that affect the rates of chemical reactions and the metabolic activity of sulfate-reducing bacteria (such as *Desulfovibrio desulfuricans*). These factors include concentration of the reactants, temperature, pressure, pH, catalysis, the organisms involved (Detmers *et al.*, 2001), and availability of nutrients such as phosphate and nitrate. A detailed discussion of the rate-controlling mechanisms of bacterial sulfate reduction is provided by Rees (1973).

The magnitude of kinetic fractionation, which can be calculated using statistical mechanics or determined from experiments, is generally smaller than that of equilibrium fractionation, and kinetic fractionation effects become smaller with increasing rates of overall reaction. Harrison and Thode (1957) determined a value of 1.024 for the k_1/k_2 ratio, which means that the H_2S produced at any instant by the reduction of SO_4^{2-} should be enriched in ^{32}S, or depleted in ^{34}S, by 24‰ relative to the remaining SO_4^{2-}. Subsequent studies have shown that the kinetic $\Delta_{SO_4^{2-}-H_2S}$ value accompanying bacterial sulfate reduction varies from 15 to 25‰ at relatively high rates of sulfate reduction to more than 60‰ at low rates of sulfate reduction (Goldhaber and Kaplan, 1975).

11.3 Stable isotope geothermometry

The isotopic fractionation factor, like the equilibrium constant, is a function of temperature and generally approaches unity at very high temperatures. Experimentally determined temperature dependence of α_{A-B} can usually be described by the following expressions:

$$\text{High } T \text{ (above about 200°C)} \qquad 1000 \ln \alpha_{A-B} \approx C_1 + \frac{C_2}{T^2}$$

$$\text{Low } T \text{ (below about 200°C)} \qquad 1000 \ln \alpha_{A-B} \approx C_3 + \frac{C_4}{T} \tag{11.24}$$

where C_1, C_2, C_3, and C_4 are empirical constants and T is in Kelvin. The temperature dependence of isotopic fractionation factors, determined experimentally, empirically, or theoretically, and expressed in the form of equations or calibration graphs, is the basis of stable isotope geothermometry. Usually, experimentally determined calibrations are more reliable, but the attainment of equilibrium in experiments at low temperatures, the

most useful range for stable isotope geothermometry, is a potential limitation. On the other hand, the magnitude of isotopic fractionations decrease rapidly with increasing temperature because of the dependence of the fractionation factor on $1/T^2$ and are generally too small at temperatures in excess of about 800°C for reliable geothermometry. A unique advantage of isotope geothermometry is that the effect of pressure on isotopic fractionation is negligible in most systems, especially at pressures less than 10 kb. This is because the volumes of isotopically substituted molecules and crystals are not sensitive to pressure changes.

The best isotope geothermometers are those for which (i) the temperature dependence of the fractionation factor is large, (ii) the fractionations between the substances under consideration are large relative to the experimental errors of isotopic analysis, and (iii) it is unlikely that the isotopic compositions of the substances have changed after their formation. Hydrogen isotope fractionations are usually large, but their relatively small temperature dependence in mineral–H_2O systems, especially below 400°C, and the ease of isotope exchange between fluids and minerals even at low temperatures preclude their use in geothermometry. Similarly, carbon isotopic fractionation among carbonate minerals is too insensitive to temperature variations to be useful in geothermometry.

Commonly used isotope geothermometry involves oxygen and sulfur isotopes. An assemblage of N oxygen-bearing or sulfur-bearing minerals in equilibrium for which calibration curves or thermometric equations are available should give, in theory, N-1 oxygen or sulfur isotopic temperatures, although all of the possible pairs will not be suitable for geothermometry. For example, the quartz–feldspar pair, a very common assemblage in felsic igneous and metamorphic rocks, is not a useful geothermometer because $\Delta^{18}O_{qz-feldspar}$ values are small and rather insensitive to temperature variation, and feldspar is particularly susceptible to post-formational isotope exchange with hydrothermal fluids.

An essential condition for reliable isotopic geothermometry is that isotopic equilibrium was achieved between phases of interest at the time of their formation and has been maintained since then. A close agreement of temperatures determined from different pairs of minerals increases the reliability of the estimated temperature and provides evidence for isotopic equilibrium among the minerals in the assemblage, indicating their formation from the same fluid at fairly uniform temperature. A lack of concordance of the temperatures usually implies a lack of isotopic equilibrium among the minerals or noncontemporaneity of one or more minerals in the assemblage, assuming that the calibrations are accurate. Another indication of a lack of isotopic equilibrium is a reversal of the commonly observed order of isotopic enrichment among coexisting phases of an assemblage. For example, the order of decreasing ^{18}O-enrichment in a granite should be quartz > feldspar > biotite > magnetite; thus, a higher $\delta^{18}O$ value for feldspar compared to quartz would indicate a disequilibrium assemblage. Generally, oxygen isotopic equilibrium among minerals in a rock is strong evidence for chemical equilibrium in the rock. The energy required to break Al–O and Si–O bonds in silicate minerals and allow rearrangement towards isotopic equilibrium is sufficient to effect chemical equilibrium (O'Neil, 1986a).

11.3.1 Oxygen isotope geothermometry

One of the earliest applications of oxygen isotope thermometry was the estimation of temperatures of ancient oceans from measurements of oxygen isotope ratios in carbonate minerals (calcite or aragonite) that constitute remains of marine organisms or limestones of known geologic age (Urey, 1947; Craig, 1965). The basis of this thermometry is that the fractionation of oxygen isotopes between calcium carbonate minerals and ocean water at any given time is a function of the water temperature. Although sound in principle, this technique has not worked well except for post-Miocene $CaCO_3$ sediments. The main limitation is that, although the $\delta^{18}O$ value of ocean water has fluctuated significantly over geologic time, the variation is not a function of temperature only. The carbonate paleothermometry is further complicated by variations in the pH of seawater (Zeebe, 2001; Royer *et al.*, 2004), post-deposition changes in the isotopic composition of the carbonate minerals, and the biochemical fractionation of oxygen by shell-forming organisms.

Silicate and oxide minerals in igneous and metamorphic rocks equilibrate at relatively higher temperatures and therefore are not saddled with complications arising from kinetic isotopic effects that occur at lower temperature equilibration typical of sedimentary rocks. As reviewed by Taylor (1997), equations describing oxygen isotopic fractionation between many mineral–H_2O pairs and mineral–mineral pairs as a function of temperature can be found in a number of publications (e.g., Clayton and Kieffer, 1991; Mathews, 1994; Zheng, 1993a,b). A set of equations (called *reduced partition functions*) of the form

$$\begin{aligned} f_{\text{mineral–H}_2\text{O}} &= 1000 \ln \alpha_{\text{mineral–H}_2\text{O}} \\ &= \text{A}_{\text{mineral}}x - \text{B}_{\text{mineral}}x^2 + \text{C}_{\text{mineral}}x^3 \end{aligned} \tag{11.25}$$

for several major rock-forming minerals relative to H_2O is listed in Table 11.2. In these equations, A, B, and C are mineral-specific constants, and $x = 10^6/T^2$ (T in Kelvin). The equations are based on a combination of laboratory experiments and statistical thermodynamic calculations, and they yield good approximations for temperatures greater than 400 K.

At a given temperature, the equilibrium oxygen isotope fractionation between any two minerals included in Table 11.2 can be computed as the algebraic difference between the two corresponding $f_{\text{mineral–H}_2\text{O}}$ functions. For example, for the mineral pair quartz (qz)–magnetite (mt), which is widely

Table 11.2 Equations ($f_{\text{mineral–H}_2\text{O}}$) for selected individual minerals for oxygen isotope geothermometry.

$$f_{\text{mineral–H}_2\text{O}} = 1000 \ln \alpha_{\text{mineral–H}_2} = A_{\text{mineral}} X - B_{\text{mineral}} X^2 + C_{\text{mineral}} X^3$$

$x = 10^6/T^2$ (T in Kelvin)

Mineral	A	B	C
Quartz	12.116	0.370	0.0123
Calcite	11.781	0.420	0.0158
Albite	11.134	0.326	0.0104
Jadeite	10.319	0.287	0.0088
Muscovite	10.221	0.282	0.0086
Anorthite	9.993	0.271	0.0082
Zoisite	9.983	0.269	0.0081
Diopside	9.237	0.199	0.0053
Garnet	8.960	0.182	0.0047
Fosterite	8.326	0.142	0.0032
Rutile	6.960	0.088	0.0017
Magnetite	5.674	0.038	0.0003

Source of data: Taylor (1997, a compilation of data from Clayton and Kieffer, 1991; Mathews, 1994; O'Neil and Taylor, 1967, 1969).
The value of 1000 ln α for any mineral–mineral pair at a given temperature is the difference between the $f_{\text{mineral–H}_2\text{O}}$ values of the two minerals. For example, for the pair quartz (qz)–magnetite (mt), $D_{\text{qz–mt}} = 1000 \ln \alpha_{\text{qz–mt}} = f_{\text{qz–H}_2\text{O}} - f_{\text{mt–H}_2\text{O}}$. At T = 1000 K, using given values of the mineral-specific constants, $1000 \ln \alpha_{\text{qz–mt}} = 11.7583 - 5.6363 = 6.122$.

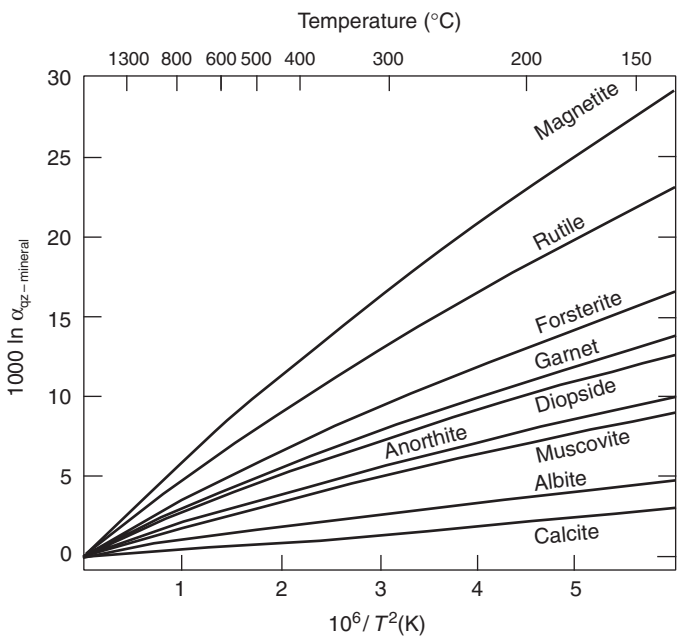

Fig. 11.2 Oxygen isotope fractionation factors between quartz and various silicate and oxide minerals as a function of temperature. The fractionation factors are all positive because at equilibrium ^{18}O is preferentially partitioned into quartz relative to all the other minerals. Calibration curves for mineral pairs were calculated directly from the respective f_{mineral} functions given in Table 11.2, as illustrated for the rutile–magnetite pair in Example 11–2.

distributed in rocks and frequently used for geothermometry (see equation 11.16),

$$\Delta_{\text{qz–mt}} = 1000 \ln \alpha_{\text{qz–mt}} = 1000 \ln \alpha_{\text{qz–H}_2\text{O}} - 1000 \ln \alpha_{\text{mt–H}_2\text{O}} \tag{11.26}$$

which can be framed in terms of $f_{\text{mineral–H}_2\text{O}}$ functions as:

$$\begin{aligned} 1000 \ln \alpha_{\text{qz–mt}} &= 1000 \ln f_{\text{qz–H}_2\text{O}} - 1000 \ln f_{\text{mt–H}_2\text{O}} \\ &= (A_{\text{qz}}x - B_{\text{qz}}x^2 + C_{\text{qz}}x^3) - (A_{\text{mt}}x - B_{\text{mt}}x^2 + C_{\text{mt}}x^3) \end{aligned} \tag{11.27}$$

where A, B, and C are mineral-specific constants, and $x = 10^6/T^2$ (T in Kelvin). For the purpose of illustration, a set of such calculated calibration curves for several minerals relative to quartz is presented in Fig. 11.2. In principle, each such calibration curve can be used to determine graphically the isotopic equilibration temperature of the mineral pair from their measured oxygen isotope ratios.

Example 11–2: Calculation of oxygen isotope thermometric equation and calibration curve for the rutile (rut)–magnetite (mt) pair based on data in Table 11.2

For the rutile (rut)–magnetite (mt) pair,

$$1000 \ln \alpha_{\text{rut–mt}} = 1000 \ln \alpha_{\text{rut–H}_2\text{O}} - 1000 \ln \alpha_{\text{mt–H}_2\text{O}} \tag{11.28}$$

Expressing in terms of $f_{\text{mineral–H}_2\text{O}}$, and incorporating the values of the coefficients as listed in Table 11.2, we obtain the thermometric equation for the rutile–magnetite pair as

$$\begin{aligned} 1000 \ln \alpha_{\text{rut–mt}} &= (A_{\text{rut}}x - B_{\text{rut}}x^2 + C_{\text{rut}}x^3) - (A_{\text{mt}}x - B_{\text{mt}}x^2 + C_{\text{mt}}x^3) \\ &= (6.960x - 0.088x^2 + 0.0017x^3) \\ &\quad - (5.674x - 0.038x^2 + 0.0003x^3) \\ &= 1.286x - 0.05x^2 + 0.0014x^3 \end{aligned} \tag{11.29}$$

where $x = 10^6/T^2$ (T in Kelvin). To construct a $1000 \ln \alpha_{\text{rut–mt}}$ versus temperature calibration curve (Fig. 11.3) for the rutile–magnetite geothermometer, we calculate $1000 \ln \alpha_{\text{rut–mt}}$ for assumed values of temperature as listed below:

$x = 10^6/T^2$	T (K)	$1000 \ln \alpha_{\text{rut–mt}}$	$x = 10^6/T^2$	T (K)	$1000 \ln \alpha_{\text{rut–mt}}$
1	1000	5.63	4	500	22.11
2	707.11	11.20	5	447.21	27.46
3	577.35	16.69	6	408.25	32.74

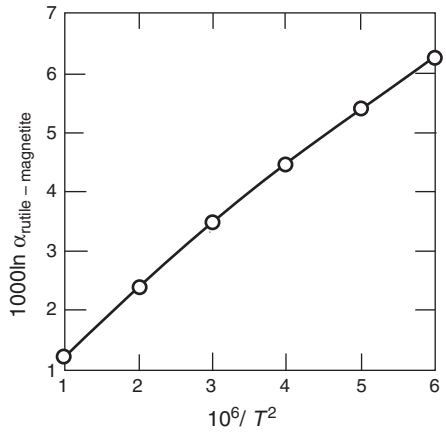

Fig. 11.3 Rutile–magnetite oxygen isotope geothermometer calculated using equations for $f_{rutile-H_2O}$ and $f_{rutile-H_2O}$ given in Table 11.2.

11.3.2 Sulfur isotope geothermometry

Equations for the commonly used sulfur isotope geothermometers, derived on the basis of a critical evaluation of the available theoretical and experimental data, are given in Table 11.3. The pyrite–galena pair is the most sensitive sulfide geothermometer, but temperatures obtained involving pyrite may show an appreciable spread because of the common occurrence of several generations of pyrite in a mineral assemblage. Sphalerite–galena is the most commonly used pair and in many cases it yields temperatures consistent with those obtained from fluid inclusion microthermometry. Inconsistent temperatures obtained from this geothermometer in some studies have been attributed to isotopic disequilibrium (Botinikov *et al.*, 1995). Even in an equilibrated assemblage, the temperature estimated may not represent the temperature of sulfide formation because sulfide minerals are prone to relatively rapid reequilibration.

11.4 Evaporation and condensation processes

Consider the fractionation of isotopes X1 and X2 in a system consisting of two substances A and B. The change in the isotopic composition of A and B with increasing fractionation will depend on the magnitude of the fractionation factor and whether the system is closed or open to A and B.To illustrate this, let us consider the fractionation of oxygen and hydrogen isotopes during evaporation of ocean water and condensation of the water vapor so formed.

Hydrogen has two stable isotopes (^1H and ^2H or D) and oxygen has three (^{16}O, ^{17}O, and ^{18}O). Thus, there are nine possible combinations for isotopically distinct water molecules, with masses ranging from 18 for $^1H_2{}^{16}O$ to 22 for $D_2{}^{18}O$. A water molecule containing the lighter isotope (^1H or ^{16}O) has a higher vibrational frequency and, therefore, weaker bonds compared to one containing the heavier isotope (D or ^{18}O) (see section 11.1.1). This results in a greater tendency of the light water molecules to escape into the vapor phase above a body of liquid water (i.e., $^1H_2{}^{16}O$ has a significantly higher vapor pressure than $D_2{}^{18}O$). Consequently, water vapor formed by evaporation of ocean water is enriched in ^{16}O and ^1H relative to the ocean water, whereas raindrops formed by condensation of water vapor are enriched in ^{18}O and D relative to the water vapor.

11.4.1 Evaporation of ocean water

Because ocean water (ow) is well mixed, it is considered to have a relatively uniform isotopic composition ($\delta D = +5$ to -7‰, $\delta^{18}O = +0.5$ to -1.0‰), with mean values very close to the defined values of the SMOW standard ($\delta D = 0$‰,

Table 11.3 Sulfur isotope geothermometers.

	Equation (T in Kelvin)	Uncertainties in the calculated temperature*	
Mineral pair in equilibrium (M1–M2)	$\Delta^{34}S = \delta^{34}S_{M1} - \delta^{34}S_{M2}$	**1**	**2**
Pyrite – galena	$T = \frac{(1.01 \pm 0.04) \times 10^3}{\sqrt{\Delta^{34}S}}$	± 25	± 20
Sphalerite (or pyrrhotite)– galena	$T = \frac{(0.85 \pm 0.03) \times 10^3}{\sqrt{\Delta^{34}S}}$	± 20	± 25
Pyrite – chalcopyrite	$T = \frac{(0.67 \pm 0.04) \times 10^3}{\sqrt{\Delta^{34}S}}$	± 35	± 40
Pyrite – sphalerite (or pyrrhotite)	$T = \frac{(0.55 \pm 0.04) \times 10^3}{\sqrt{\Delta^{34}S}}$	± 40	± 55

*1 = Uncertainty in estimated temperature from uncertainty in the equation (at 300°C).
2 = Uncertainty from the analytical uncertainty of ± 0.2‰ for Δ values (at 300°C).
Source of data: Ohmoto and Rye (1979).

$\delta^{18}O = 0‰$). Larger variations exist, but only in special situations, such as seas in arid regions with restricted access to the open ocean.

For all practical purposes, the ocean is an infinite reservoir of water with constant $\delta^{18}O$ and δD values, which do not change because of evaporation of a very small fraction of the reservoir to water vapor (wv) or addition of a relatively small volume of meteoric water by rivers and precipitation. Thus, the ocean water is considered to be an open system with respect to liquid water. The system is also open with respect to water vapor because it escapes to the atmosphere as soon as it is formed instead of staying in equilibrium with water.

The values of isotopic fractionation factors for evaporation of water under equilibrium conditions at 25°C (298.15 K) are (Dansgaard, 1964):

$$\alpha^{ox}_{ow-wv} = \frac{(^{18}O/^{16}O)_{ow}}{(^{18}O/^{16}O)_{wv}} = 1.0092 \tag{11.30}$$

$$\alpha^{hy}_{ow-wv} = \frac{(D/H)_{ow}}{(D/H)_{wv}} = 1.074 \tag{11.31}$$

That the fractionation factor for both oxygen and hydrogen isotopes is > 1 is consistent with our expectation that the ocean water would be enriched in the heavier isotopes relative to water vapor. The values of $\delta^{18}O_{wv}$ and δD_{wv} at 25°C (298.15 K can be calculated using equation (11.10):

$$\alpha^{ox}_{ow-wv} = \frac{\delta^{18}O_{ow} + 1000}{\delta^{18}O_{wv} + 1000} = \frac{0 + 1000}{\delta^{18}O_{wv} + 1000}$$

$$\delta^{18}O_{wv} = \frac{1000}{\alpha^{ox}_{ow-wv}} - 1000 = \frac{1000}{1.0092} - 1000 = -9.12‰ \tag{11.32}$$

Similarly,

$$\delta D_{wv} = \frac{1000}{\alpha^{hy}_{ow-wv}} - 1000 = \frac{1000}{1.074} - 1000 = -68.90‰ \tag{11.33}$$

Deviations from these values in the open oceans are usually attributed to kinetic isotopic effects (Craig and Gordon, 1965).

11.4.2 Condensation of water vapor

The process of condensation of water vapor is the reverse of evaporation of ocean water. In contrast to ocean water, however, a mass of water vapor in the atmosphere is not a reservoir of constant isotopic composition. As condensation is dominantly an equilibrium process, the isotopic composition of the first raindrops falling out of a new mass of water vapor ($\delta^{18}O_{wv} = -9.12$; $\delta D_{wv} = -68.90$) over the ocean is very close to that of ocean water ($\delta^{18}O_{ow} \approx 0$; $\delta D_{ow} \approx 0$). However, the continuing preferential removal of ^{18}O and D from a mass of water vapor into liquid water causes the remaining water vapor to be progressively enriched in ^{16}O and ^{1}H (and depleted in ^{18}O and D). This, in turn, causes the rainwater in equilibrium with the water vapor to become progressively depleted in ^{18}O and D as well.

Thus, the water vapor (wv)–rainwater (rw) system is closed to the parent (wv), but open to the product species (rw) in the sense that it is continuously removed from the system. Isotopic fractionation in such a system can be modeled by the *Rayleigh distillation equation* (see also section 12.3.3):

$$R = R_0 \, f^{(\alpha_{rw-wv} - 1)} \tag{11.34}$$

where R_0 is the initial $^{18}O/^{16}O$ or D/H ratio of the water vapor, R is the $^{18}O/^{16}O$ or D/H ratio of the remaining water vapor after precipitation, f is the atomic fraction of the water vapor remaining in the system with respect to the original amount at any particular extent of evolution of the system (i.e., $f_{wv} = 1$ at the beginning condensation and $f_{wv} = 0$ when all the water vapor has rained out), and α_{rw-wv} is the rainwater (product)–water vapor (parent) fractionation factor (i.e., $\alpha_{rw-wv} = R_{rw}/R_{wv}$).

Equations for calculating the oxygen and hydrogen isotopic compositions of the remaining water vapor and the rainwater in equilibrium with that vapor as a function of f are (see Box 11.2):

For oxygen isotopes,

$$\delta^{18}O^{remaining}_{wv} = (\delta^{18}O^{initial}_{wv} + 1000) f^{(\alpha_{rw-wv} - 1)}_{wv} - 1000 \tag{11.35}$$

$$\delta^{18}O_{rw} = (\delta^{18}O^{remaining}_{wv} + 1000)\ \alpha_{rw-wv} - 1000 \tag{11.36}$$

For hydrogen isotopes,

$$\delta D^{remaining}_{wv} = (\delta D^{initial}_{wv} + 1000) f^{(\alpha_{rw-wv} - 1)}_{wv} - 1000 \tag{11.37}$$

$$\delta D_{rw} = (\delta D^{remaining}_{wv} + 1000)\ \alpha_{rw-wv} - 1000 \tag{11.38}$$

Calculations of $\delta^{18}O^{remaining}_{wv}$ and $\delta^{18}O_{rw}$ as a function of f_{wv} are presented in Example 11-3 and the results are shown in Fig. 11.4.

Box 11.2 Equations for the oxygen and hydrogen isotopic compositions of rainwater and remaining water vapor as a function of progressive condensation at constant temperature

In essence, the exercise involves expressing R and R_0 in equation (11.34) in terms of δ values. For oxygen isotopes, expressions for R and R_0 from equation (11.9) are:

$$R_{0\,(\mathrm{wv})} = \left(\frac{\delta^{18}\mathrm{O}_{\mathrm{wv}}^{\mathrm{initial}} + 1000}{1000}\right) R_{\mathrm{std}};\ R_{\mathrm{wv}} = \left(\frac{\delta^{18}\mathrm{O}_{\mathrm{wv}}^{\mathrm{remaining}} + 1000}{1000}\right) R_{\mathrm{std}} \tag{11.39}$$

Dividing,

$$\frac{R_{(\mathrm{wv})}}{R_{0\,(\mathrm{wv})}} = \frac{\delta^{18}\mathrm{O}_{\mathrm{wv}}^{\mathrm{remaining}} + 1000}{\delta^{18}\mathrm{O}_{\mathrm{wv}}^{\mathrm{initial}} + 1000} = f_{\mathrm{wv}}^{(\alpha_{\mathrm{rw-wv}} - 1)}$$

where f_{wv} is the fraction of the water vapor remaining, and $\alpha_{\mathrm{rw-wv}}$ is the rainwater (rw)–water vapor (wv) fractionation factor (i.e., $\alpha_{\mathrm{rw-wv}} = R_{\mathrm{rw}}/R_{\mathrm{wv}}$). Rearranging, we get the equation to calculate the δ^{18}O value of the remaining water vapor for a given value of f_{wv}:

$$\delta^{18}\mathrm{O}_{\mathrm{wv}}^{\mathrm{remaining}} = (\delta^{18}\mathrm{O}_{\mathrm{wv}}^{\mathrm{initial}} + 1000) f_{\mathrm{wv}}^{(\alpha_{\mathrm{rw-wv}} - 1)} - 1000 \tag{11.35}$$

The corresponding δ^{18}O value of rainwater can be obtained from the definition of $\alpha_{\mathrm{rw-wv}}$:

$$\alpha_{\mathrm{rw-wv}} = \frac{R_{\mathrm{rw}}}{R_{\mathrm{wv}}^{\mathrm{remaining}}} = \frac{\delta^{18}\mathrm{O}_{\mathrm{rw}} + 1000}{\delta^{18}\mathrm{O}_{\mathrm{wv}}^{\mathrm{remaining}} + 1000}$$

Rearranging the terms, we get

$$\delta^{18}\mathrm{O}_{\mathrm{rw}} = (\delta^{18}\mathrm{O}_{\mathrm{wv}}^{\mathrm{remaining}} + 1000)\ \alpha_{\mathrm{rw-wv}} - 1000 \tag{11.36}$$

Equations for $\delta\mathrm{D}_{\mathrm{wv}}^{\mathrm{remaining}}$ (equation 11.37) and $\delta\mathrm{D}_{\mathrm{rw}}$ (equation 11.38) can be derived in a similar manner.

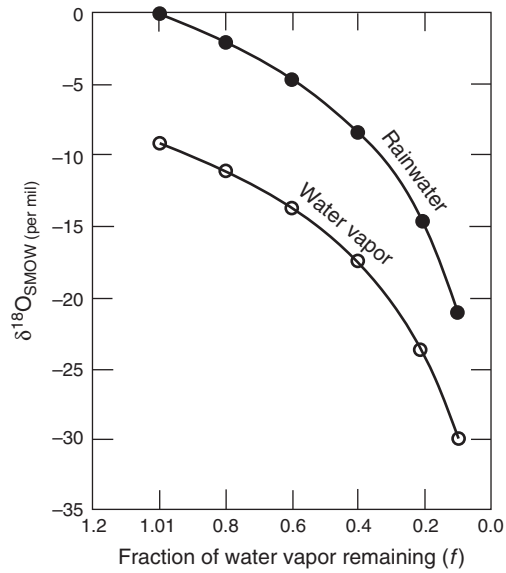

Fig. 11.4 Variation of δ^{18}O in course of condensation of water vapor ($\delta^{18}\mathrm{O}_{\mathrm{wv}}^{\mathrm{initial}} = -9.1$) at 25°C, according to Rayleigh distillation equation. $\alpha_{\mathrm{rw-wv}} = 1.0092$. The δ^{18}O value of the first condensate is taken as 0.0. The δ^{18}O value of rainwater is negative irrespective of what fraction of the water vapor condenses, and it becomes increasingly more negative as the condensation progresses.

Example 11–3: Calculation of the progressive change in d18O (water vapor) and in the corresponding d18O (rainwater) at 25°C (298.15 K)

Let us accept that the initial δ^{18}O value of the water vapor is 9.1‰ and $\alpha_{\mathrm{rw-wv}} = 1.0092$ at 25°C. For any chosen value of f_{wv} ($f_{\mathrm{wv}} \leq 1$), we can calculate $\delta^{18}\mathrm{O}_{\mathrm{wv}}^{\mathrm{remaining}}$ using equation (11.35) and $\delta^{18}\mathrm{O}_{\mathrm{rw}}$ using equation (11.36). The results are tabulated below (Table 11.4) and presented in the form of graphs in Fig. 11.4.

Note that the δ^{18}O value of rainwater is negative irrespective of what fraction of the water vapor condenses, and it becomes increasingly more negative with increased condensation, which accounts for the fact that δ^{18}O values of meteoric waters (water recently involved in atmospheric circulation)

Table 11.4 Progressive change in δ^{18}O (water vapor) and in the corresponding δ^{18}O (rainwater) at 25°C (298.15 K) with increasing precipitation.

Fraction of water vapor remaining (f_{wv})	$\delta^{18}\mathrm{O}_{\mathrm{wv}}^{\mathrm{remaining}}$ (per mil)	$\delta^{18}\mathrm{O}_{\mathrm{rw}}$ (per mil)	Fraction of water vapor remaining (f_{wv})	$\delta^{18}\mathrm{O}_{\mathrm{wv}}^{\mathrm{remaining}}$ (per mil)	$\delta^{18}\mathrm{O}_{\mathrm{rw}}$ (per mil)
1.0	–9.1	0.0	0.5	–15.4	–6.4
0.9	–10.1	–1.0	0.4	–17.4	–8.4
0.8	–11.2	–2.1	0.3	–20.0	–11.0
0.7	–12.4	–3.3	0.2	–23.7	–14.7
0.6	–13.8	–4.7	0.1	–29.9	–21.0

are negative compared with ocean water. Similar calculations will show that δD values of meteoric waters are also negative relative to ocean water.

11.4.3 Meteoric water line

Because isotopic fractionation increases with decreasing temperature, δD and δ^{18}O values of meteoric water vary with latitude and elevation: the higher the latitude or the elevation, the more depleted is the meteoric water in ^{18}O and D. δ^{18}O values of less than −50‰ and δD values of less than −450‰ have been measured at the South Pole. The D/H fractionation, however, is proportional to the ^{18}O/^{16}O fractionation because condensation of H_2O in the Earth's atmosphere is essentially an equilibrium process. Thus, in a δD versus δ^{18}O plot, all meteoric waters around the globe fall close to a straight line (Fig. 11.5), called the *global meteoritic water line* (GMWL), which is defined by the equation (Craig, 1961):

$$\delta D = 8\,\delta^{18}O + 10 \tag{11.40}$$

The intercept of +10‰ for the GMWL is a consequence of the nonequilibrium evaporation process and is the reason why ocean water does not fall on the GMWL line. If evaporation were an equilibrium process, the intercept would be zero. Surface waters that have been affected by evaporation, hydration, or interaction with silicate and carbonate minerals may deviate from the global meteoric water line. For any location on the globe, we can establish a *local meteoric water line* (LMWL) by analyzing the isotope ratios of local precipitation (rain and snow) over a period of time. Equation (11.40), however, satisfactorily describes the slope and intercept of the meteoric water line on a global scale. The value of the intercept can vary substantially from one locality to another, mainly because of variability in evaporation; the slope of the meteoric water line is very close to 8.0 for all precipitation that has not experienced isotopic fractionation subsequent to condensation.

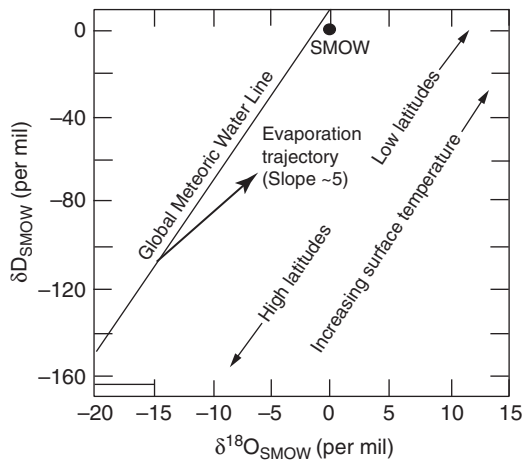

Fig. 11.5 A δD versus δ^{18}O plot showing the global meteoric water line (GMWL) as defined by equation (11.40) and a typical trajectory for deviations from the GMWL.

11.5 Source(s) of water in hydrothermal fluids

The term "hydrothermal fluid" refers to naturally occurring aqueous fluids involved in the dissolution, precipitation, and alteration of minerals. The waters of hydrothermal fluids may be classified into four end-member categories: (i) *meteoric* – water recently involved in atmospheric circulation (e.g., rainwater, water in rivers and lakes, ocean water); (ii) *connate* – formation water trapped in pores of sediments deposited in an aqueous environment; (iii) *metamorphic* – water produced by metamorphic dehydration reactions or water that equilibrated with metamorphic rocks at temperatures above about 300°C; and (iv) *magmatic* – water derived from magma, regardless of the ultimate source of the water.

A combination of ^{18}O/^{16}O and D/H ratios has proved very useful in tracing the origin and evolution of hydrothermal fluids, including fluids responsible for the formation of ore deposits (Taylor, 1974, 1997; Sheppard, 1986). ^{18}O/^{16}O and D/H ratios are affected somewhat differently in water–rock systems. Because of the extremely small amount of hydrogen in rocks (usually < 2000 ppm), the D/H ratio of a fluid undergoes negligible change by mineral–water exchange reactions. In contrast, the ^{18}O/^{16}O ratio of the fluid may be modified significantly unless water : rock ratios are very high or the isotopic exchange reactions are ineffective for kinetic or other reasons. The magnitude of the shift, which is generally to higher δ^{18}O values because of the water evolving towards oxygen isotopic equilibrium with ^{18}O–rich silicate and carbonate minerals, is determined by: (i) the ratio of the amount of oxygen in the exchangeable minerals to that in the fluid; (ii) the magnitude of mineral–H_2O fractionation factors (which takes into account the temperature of isotopic exchange); and (iii) the initial isotopic composition of the reacting minerals. Thus, the D/H ratio of a hydrothermal fluid is a better indicator of the source of the fluid, whereas its ^{18}O/^{16}O ratio may provide information about its subsequent evolution.

Two methods are used to determine D/H and ^{18}O/^{16}O ratios of hydrothermal fluids. Direct measurements are possible only in cases where the fluids can be sampled directly, such as connate brines, geothermal waters, and fluid inclusions. Isotopic compositions of fluids that are not amenable to direct sampling, as in the case of igneous and metamorphic rocks, are determined indirectly from mineral assemblages presumed to have been in equilibrium with the fluid. In essence, the indirect method involves the following steps: isotopic analysis of mineral assemblages, estimation of temperature of formation utilizing appropriate geothermometers, and calculation of D/H and ^{18}O/^{16}O ratios of fluids in equilibrium with assemblages at temperatures of their formation using appropriate mineral–H_2O fractionation factors. The uncertainty in δD and δ^{18}O values of fluids estimated by the indirect method arises largely from uncertainties in the temperatures of mineral deposition and in the values of isotopic fractionation factors. The indirect method is more commonly

used, especially for $^{18}O/^{16}O$ ratios, because it is technically much easier. Because of the paucity of hydrogen-bearing minerals in many ore deposits, fluid inclusion analysis usually is the only direct method for obtaining information on the δD values of ore-forming fluids. The accuracy of determination of δD is typically an order of magnitude worse than for $\delta^{18}O$ (typically ±1.0‰ versus ±0.1‰). However, the natural variations in D/H are also much larger than for $\delta^{18}O$; so a 10‰ variation generally represents a very large $\delta^{18}O$ change but only a small δD change.

If the oxygen and hydrogen isotopic compositions and temperature of ancient ocean waters were comparable to present-day values, then ancient meteoric waters would be expected to follow a relation similar to GMWL. The variation of ocean water isotopic composition through geologic time is not known with any certainty, but indications are that their composition has been essentially the same at least during the Cenozoic and the Mesozoic (±1‰ for $^{18}O/^{16}O$ and ±10‰ for D/H) and possibly as far back as the Lower Paleozoic (Knauth and Roberts, 1991). $^{18}O/^{16}O$ ratios of ancient cherts suggest that Precambrian ocean water was depleted in ^{18}O by up to 20‰ (Perry 1967), but other studies have concluded that the $\delta^{18}O$ values of the ocean waters have remained relatively constant throughout much of the Proterozoic (Holmden and Muehlenbachs 1993), and even during the Archean (Gregory and Taylor, 1981; Beaty and Taylor, 1982; Gregory, 1991). Discussing the various approaches that have been used to resolve this question, Sheppard (1986) proposed that the isotopic compositions of ancient ocean waters, at least since about 2500 Ma, have stayed within narrow limits of about 0 to −3‰ for $\delta^{18}O$ and about 0 to −25‰ for δD, not radically different from their present-day values. Also, modeling of the interaction between oceanic crust and ocean water, the dominant process for regulating the oxygen isotope composition of the oceans (Muehlenbachs and Clayton, 1976), indicates that the $\delta^{18}O$ value of ocean water may vary by ±2‰, with a time response ranging from 5 to 50 Myr for mid-oceanic ridge expansion rates of 110 cm per year (Lécuyer and Allemand, 1999). Thus, it appears reasonable to use the present-day GMWL as a reference for evaluating fossil hydrothermal systems.

The isotopic compositions of different kinds of natural waters are summarized in Fig. 11.6. Most volcanic and plutonic igneous rocks have very uniform $\delta^{18}O$ values (+ 5.5 to +10.0‰) and δD values (−50 to −85‰); the field shown as "primary magmatic water" corresponds to the calculated isotopic composition of water in equilibrium with such normal igneous rocks at $t \geq$ 700°C. The field of metamorphic water also represents calculated values for waters in equilibrium with metamorphic minerals at t=300° to 600°C. Evidently, the fields for magmatic and metamorphic waters shown in Fig. 11.6 are approximate. The *kaolinite line* in Fig 11.6 represents the locus of isotopic data points for pure kaolinites from weathering zones formed in approximate equilibrium with meteoric water at surface temperatures (Savin and Epstein, 1970). It is parallel to the meteoric

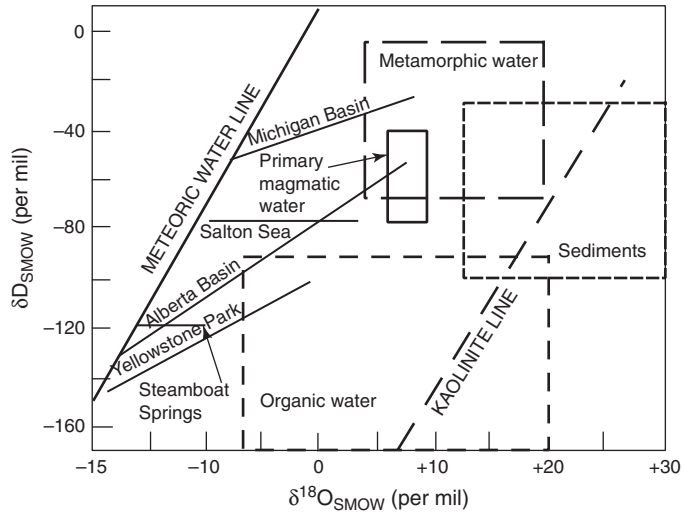

Fig. 11.6 Oxygen and hydrogen isotopic compositions of various hydrothermal waters relative to the SMOW standard. The global meteoric water line (GMWL) defines the compositions of meteoric water; the kaolinite line represents the isotopic compositions of kaolinites formed by chemical weathering. Also shown are trends for the Michigan Basin, the Alberta Basin, and the Yellowstone Park (Wyoming) geothermal brines, and the $\delta^{18}O$ shifts of the geothermal waters of Steamboat Springs (Nevada) and Salton Sea (California) relative to the isotopic composition of present-day meteoric water in these areas. (Sources of data: Taylor, 1974; White, 1974; Sheppard, 1986.)

water line, shifted in $\delta^{18}O$ and δD value by about 27‰ and 30‰, respectively, from the local meteoric water. The kaolinite line is potentially useful for discriminating clay minerals formed by chemical weathering from those formed by hydrothermal alteration. However, the interpretation of variations in clay mineral isotopic data is rather complicated because clay minerals may be composed of a mixture of detrital and authigenic components, and because particles of different ages may have exchanged isotopes to varying degrees (Hoefs, 1997).

Analyses of waters from active geothermal systems around the world have shown that these waters essentially are of local meteoric derivation. Some examples are shown in Fig. 11.6. In almost all cases, the hot water or steam shows a characteristic shift to higher $\delta^{18}O$ values as a result of isotopic exchange with silicate and carbonate minerals of the country rocks. In contrast, because of the extremely small initial hydrogen content of the rocks relative to the amounts of water involved, the δD values either remain almost identical to local meteoric waters (e.g., Steamboat Springs, Nevada, USA) or show a linear increase compared with local meteoric waters because of evaporation (e.g., Yellowstone Park, Wyoming, USA). Meteoric water is considered to be the main, if not the only, source of recharge for the Salton Sea geothermal brines, California (Craig, 1966; Clayton *et al.*, 1968). The 1.5 to 2‰ higher $\delta^{18}O$ in these waters relative to the meteoric water line is probably because of evaporation of meteoric waters in the desert environment prior to infiltration (White, 1974). On the

basis of δD versus δ^{18}O trends, oilfield brines (formation waters), once thought to represent connate waters (seawater trapped in sediments), are now believed to contain a major component of circulating meteoric groundwater. Similar to surface meteoric waters, oilfield brines show a general increase in δD and, to a lesser extent, in δ^{18}O toward lower latitudes (e.g., the Michigan Basin brines versus the Alberta Basin brines, Fig. 11.6). Within a given sedimentary basin, however, the δD values generally increase with increasing δ^{18}O (and salinity). According to Taylor (1974) this trend is a result of one or more of the following processes: mixing of meteoric waters with waters of connate or other origin; isotopic exchange with clay minerals in the rocks; fractionation effects by processes such as membrane filtration; and reactions involving petroleum hydrocarbons.

11.6 Estimation of water: rock ratios from oxygen isotope ratios

Interaction of rocks with hydrothermal fluids results in a shift in δ^{18}O values, which can be used to estimate the water: rock ratio in the system during the alteration. The basis of this exercise is the mass balance equation pertaining to oxygen isotopes (Taylor, 1977, 1979):

$$w\delta^{i}_{\text{water}} + r\delta^{i}_{\text{rock}} = w\delta^{f}_{\text{water}} + r\delta^{f}_{\text{rock}} \tag{11.41}$$

The superscripts i and f refer, respectively, to the initial state (i.e., before water–rock interaction) and the final state (i.e., after interaction), w is the atom percent of meteoric water oxygen in the rock + water system, and r is the atom percent of exchangeable rock oxygen in the rock + water system.

Let us first consider the simplest model, a "closed" system in which the water is recyled over and over again through the rock until the rock attains the equilibrium value δ^{f}_{rock} at a certain temperature and then expelled from the system, and $\delta^{f}_{\text{water}}$ is determined by isotopic equilibration with the rock. The material-balance water: rock ratio (w/r) for this ideal "closed" system, integrated over its lifetime, can be calculated from the following relationship derived by rearranging equation (11.41):

$$\left(\frac{w}{r}\right)_{\text{closed}} = \frac{\delta^{f}_{\text{rock}} - \delta^{i}_{\text{rock}}}{\delta^{i}_{\text{water}} - (\delta^{f}_{\text{rock}} - \Delta_{r-w})} \tag{11.42}$$

where $\Delta_{r-w} = \delta^{f}_{\text{rock}} - \delta^{f}_{\text{water}}$ at the temperature of equilibration. This is the theoretical w/r ratio; the actual w/r ratio may be different depending on the efficiency of the exchange reaction.

At the other extreme is the "open" system model in which each infinitesimal packet of water makes only a single pass through the system and does not recycle. The equation for the integrated w/r ratio in this case is (Taylor, 1977):

$$\left(\frac{w}{r}\right)_{\text{open}} = \ln\left[\frac{\delta^{i}_{\text{water}} + \Delta_{r-w} - \delta^{i}_{\text{rock}}}{\delta^{i}_{\text{water}} - (\delta^{f}_{\text{rock}} - \Delta_{r-w})}\right] = \ln\left[1 + \left(\frac{w}{r}\right)_{\text{closed}}\right] \tag{11.43}$$

Note that for a given set of initial conditions and constant w/r ratio, δ^{f}_{rock} is determined solely by Δ_{r-w}, which is a function of temperature only. Conversely, for a given set of initial values and constant temperature, δ^{f}_{rock} is determined only by the w/r ratio. For both closed and open systems, we can calculate the w/r ratios as a function of δ^{f}_{rock} and temperature (for more details, see Taylor, 1977; Gregory *et al.*, 1989; Larson and Zimmerman, 1991; Nabelek, 1991). Both the models give minimum values of w/r ratio, because an appreciable amount of water may have moved through fractures in the rock without exchanging oxygen isotopes.

Uncertainties in the results obtained using equations (11.42) and (11.43) arise from the fact that several of the variables in them cannot be measured and, therefore, have to be estimated. δ^{i}_{rock} is estimated either on the basis of experience with similar rock types or from measured values of a sample far removed from the effects of hydrothermal alteration; $\delta^{i}_{\text{water}}$ is estimated either from the paleogeographic reconstruction of meteoritic water values or from a range of assumed values; and Δ_{r-w} from temperature of equilibration determined by some method of geothermometry. Moreover, because of the common lack of isotopic equilibrium among the various minerals of a rock, especially at low temperatures, we should calculate a separate w/r ratio for each mineral, and then combine these with modal abundances to calculate a bulk w/r ratio for the rock. A common practice for the sake of convenience is to assume that $\delta^{18}O^{f}_{\text{rock}}$ at equilibrium is equal to the $\delta^{18}O^{f}$ value of plagioclase feldspar, and calculate $\Delta^{18}O_{r-w}$ utilizing the plagioclase feldspar–H_2O geothermometer (O'Neil and Taylor, 1967):

$$1000 \ln \alpha_{\text{plag-water}} = \Delta^{18}O_{\text{plag-water}} = -3.41 - 0.41\,\text{An} + (2.91 - 0.76\,\text{An})\left(\frac{10^6}{T^2}\right) \tag{11.44}$$

where An denotes the anorthite content of the plagioclase expressed as mole fraction, and T is the temperature of equilibration in Kelvin. This is a reasonable simplification because plagioclase is an abundant mineral in most rocks, and it exhibits the greatest rate of ^{18}O exchange with an external fluid phase.

Because the hydrogen concentration of a rock is only a fraction of the oxygen concentration, interaction with hydrothermal solution affects the isotopic composition of hydrogen much more strongly than that of oxygen. Even for very low w/r ratios, the δ D values of the hydrous minerals change rapidly, while δ^{18}O values remain essentially unchanged. Appreciable change in δ^{18}O values occurs only when w/r ratios become quite high, by which time hydrogen in the hydrous phases would have completely equilibrated with the infiltrating fluid.

Example 11–4: Calculation of the water : rock ratio for a hydrothermally altered igneous body from the given oxygen isotope data, assuming that $\delta^{18}O^f_{rock}$ at equilibrium is equal to the $\delta^{18}O$ value of plagioclase (An_{30}) and 500°C is the temperature of isotopic equilibration.
$\delta^{18}O^i_{rock}$=+ 6.5‰; $\delta^{18}O^f_{rock}$=–4‰; and $\delta^{18}O^i_{water}$=–14 ‰

Substituting values in the plagioclase (An_{30})–H_2O geothermometer of O'Neil and Taylor (1967), equation (11.44) yields:

$$\Delta^{18}O_{plag-water}(\text{at } 500^{o}C) = -3.41 - (0.41 \times 0.30) + [2.91 - (0.76 \times 0.30)]\left(\frac{10^6}{(500+273)^2}\right) = -3.533 + (2.682 \times 1.674) = 0.956$$

Assuming $\delta^{18}O_{plag} \approx \delta^{18}O^f_{rock}$, $\Delta^{18}O_{rock-water} = \Delta^{18}O_{plag-water} = 0.956$

For closed system:

$$\left(\frac{w}{r}\right)_{closed} = \frac{\delta^{18}O^f_{rock} - \delta^{18}O^i_{rock}}{\delta^{18}O^i_{water} - (\delta^{18}O^f_{rock} - \Delta^{18}O_{r-w})} = \frac{-4.0 - 6.5}{-14 - (-4 - 0.956)} = 1.16$$

For open system: $$\left(\frac{w}{r}\right)_{open} = \ln\left[1 + \left(\frac{w}{r}\right)_{closed}\right] = \ln[1 + 1.16] = 0.77$$

$$\delta^{18}O^f_{water} = \delta^{18}O^f_{rock} - \Delta^{18}O_{r-w} = -4 - 0.956 = -4.956 \text{ ‰}$$

Thus, a decrease in $\delta^{18}O_{rock}$ from +6.5‰ to –4‰ is compensated by an increase in $\delta^{18}O_{water}$ from –14‰ to –4.96‰ for maintaing mass balance in the rock–water system.

11.7 Sulfur isotopes in sedimentary systems

There are two major reservoirs of sulfur on the Earth that have uniform sulfur isotopic compositions: the mantle, which has $\delta^{34}S \approx 0$‰ and in which sulfur is present primarily in the reduced form as sulfide (H_2S); and seawater, which has $\delta^{34}S$=+ 20‰ (at the present time) and in which sulfur is present in the oxidized form as dissolved sulfate (SO_4^{2-}). The main source of H_2S for the precipitation of sulfides in sediments is the reduction of dissolved seawater SO_4^{2-} by organic matter. Dissolved SO_4^{2-} may also be derived from connate water, and/or dissolution of sulfate minerals (mainly gypsum and anhydrite). The major sources of organic matter in sediments are crude oil, thermogenic natural gas and/or gas condensates, and microbial methane. A generalized, overall reaction for the reduction of sulfate by organic matter, which is accompanied by the oxidation of organic carbon, may be written as:

$$SO_4^{2-} + 2CH_2O \Rightarrow H_2S + 2HCO_3^- \quad (11.45)$$

where the organic matter is approximated as CH_2O. The reducing agent could also be H_2 or CH_4 generated by the breakdown of organic matter:

$$SO_4^{2-} + 2H^+ + 4H_2 \Rightarrow H_2S + 4H_2O \quad (11.46)$$

$$SO_4^{2-} + CH_4 \Rightarrow H_2S + CO_3^{2-} + H_2O \quad (11.47)$$

The sulfate reduction is either catalyzed by anaerobic, sulfate-reducing bacteria at relatively low temperatures and is referred to as *bacterial sulfate reduction* (BSR), or it occurs at relatively elevated temperatures without the involvement of bacteria and is referred to as *thermochemical sulfate reduction* (TSR). In either case, the product H_2S becomes enriched in ^{32}S relative to the parent SO_4^{2-} and the parent in ^{34}S relative to H_2S. The major reaction products and byproducts by BSR and TSR are identical. However, as discussed by Machel *et al.* (1995), petrographic, isotopic, and compositional data of these products and byproducts may permit identification of a BSR versus a TSR origin of the H_2S.

In most marine sediments, 75% to 90% of the H_2S (or HS^-, depending on the pH) produced by SO_4^{2-} reduction is reoxidized by reaction with dissolved oxygen in overlying porewater, or with Fe(III) or Mn(IV) within the sediment. The rest is incorporated in the sediment as sulfide minerals, predominantly as pyrite (FeS_2) by way of iron "monosulfide" precursors (with stoichiometry close to FeS), during early diagenesis when the sediments are still within about 1 m of the seawater–sediment interface, as long as the sediments contain enough reactive iron. When the supply of reactive iron is exhausted, H_2S (or HS^-) combines with organic matter to form organosulfur compounds. In typical shales, 10 to 30% of the reduced sulfur in sediments is fixed as organic sulfur and the rest as pyrite; in Fe-poor hosts, such as carbonate sediments, organically bound sulfur usually exceeds pyrite sulfur by a factor of more than two (Dinur *et al.*, 1980). The $\delta^{34}S$ value of organic sulfur tends to be higher than the coexisting pyrite by 1 to 10‰, and organic matter within a given stratigraphic unit may have a distinct $\delta^{34}S$ signature that would permit the use of sulfur species in identifying the source rocks and the migration paths of petroleum (Dinur *et al.*, 1980; Thode, 1981). In general, bacterial sulfate reduction is limited by the availability of metabolizable organic carbon, which typically amounts to about 15–45% of the total organic carbon in the sediment. Commonly, this relationship is reflected by a positive correlation between organic carbon and pyrite-bound sulfur in normal marine sediments (Goldhaber and Kaplan, 1975; Berner, 1985):

$$\text{Pyrite S (wt\%)} = 0.37 \times \text{organic carbon (wt\%)} \quad (11.48)$$

If the observed S : C mass ratio in the sediment is much greater than 1, diagenetic sulfide precipitation may not be the only or even the dominant source of sulfur in the sediment.

The $\delta^{34}S$ value of H_2S generated by sulfate reduction is determined by several factors: (i) the initial isotopic composition of the seawater sulfate; (ii) the mechanism of reduction (BSR or TSR) and factors affecting such reduction; (iii) the kind of sedimentary system (open or closed to SO_4^{2-} and/or H_2S); and (iv) oxidation of sulfides. Fractionation of sulfur isotopes associated with pyrite formation from dissolved sulfide in the laboratory has been reported to be less than 1‰ (Price and Shieh, 1979). Thus, for all practical purposes, sulfide minerals precipitated by reaction of metal complexes with H_2S, an important process in the formation of sulfide deposits in sedimentary environments, inherit the sulfur isotopic composition of H_2S.

11.7.1 Bacterial sulfate reduction (BSR)

Sulfur is an essential, although minor, constituent of living cells. A large and diverse group of microorganisms assimilate sulfur from the environment, most commonly as sulfate (but sometimes as sulfide or even as thiosulfate, polythionates and elemental sulfur), which is then reduced to sulfide for incorporation into the principal organosulfur compounds within cells. In this process, usually H_2S is not produced from sulfate in detectable amounts, except as a transient intermediate. This metabolic pathway, which requires input of energy, is known as *assimilatory sulfate reduction*, a complex biochemical process that generally is associated with small sulfur isotope fractionations, $\Delta^{34}S_{\text{sulfate—organic sulfur}}$ ($= 1000 \ln \alpha_{\text{sulfate—organic sulfur}} \approx \delta^{34}S_{\text{sulfate}} - \delta^{34}S_{\text{organic—S}}$) being in the order of 3‰ (Canfield, 2001b). A much smaller, specialized group of microorganisms (prokaryotes), who gain energy for their growth by catalyzing thermodynamically favorable reactions such as (11.45) and (11.46), reduces sulfate in great excess of nutritional requirements and produces H_2S depending on the amount of organic material or H_2 dissimilated. This process of reduction of sulfate to sulfide is termed *dissimilatory sulfate reduction*, which is associated with large kinetic fractionations, the $\Delta^{34}S_{\text{sulfate—sulfide}}$ ($\approx \delta^{34}S_{\text{sulfate}} - \delta^{34}S_{\text{sulfide}}$) values ranging up to 46‰ (see section 11.2.2).

Sulfate-reducing bacteria, which utilize sulfate as a terminal electron acceptor to oxidize organic matter and produce H_2S, appear to have been active as early as ~3.47 Ga (Shen *et al.*, 2001). The bacteria are an ecologically diverse group and tend to develop wherever sulfate is present and the supply and decomposition of organic matter are sufficient to create anaerobic conditions (Trudinger *et al.*, 1985). The organisms, or evidence of their activities, have been detected in anoxic environments ranging in temperatures from −1.5°C to just over 100°C and ranging in salinities from freshwater to near halite saturation. Most of the described sulfate-reducers are mesophilic bacteria, which can tolerate temperatures from near 0°C to a maximum of about 40° to 60°C. At low temperatures (< 60°C), BSR is perhaps the only effective mechanism of sulfate reduction. The upper temperature limit of BSR has not been established experimentally, but empirical evidence indicates an upper limit of about 60° to 80°C, above which almost all sulfate-reducing bacteria cease to metabolize (Machel *et al.*, 1995). In general, individual sulfate reducers can metabolize only within a narrow temperature range of 20° to 40°C, and organisms with different temperature adaptation fractionate similarly. The wide range of temperatures over which BSR occurs in nature results from the involvement of a variety of organisms with overlapping temperature adaptations (Canfield, 2001a).

The major organisms known to be dissimilatory sulfate reducers are species of *Desulfovibrio*, especially *Desulfovibrio desulfuricans,* and certain Clostridia. Studies on sulfate reducers, largely based on *Desulfovibrio desulfuricans*, have led to the following general observations pertaining to sulfur isotope fractionations by BSR (Canfield, 2001b; Canfield *et al.*, 2006).

(1) When organisms utilize organic electron donors, the extent of fractionation tends to vary inversely as the specific rate of sulfate reduction. According to Goldhaber and Kaplan (1975), the ratio k_1/k_2 (see reaction 11.23) increases from 1.015–1.025 at relatively high rates of sulfate reduction to more than 1.065 at low rates of sulfate reduction. The value of 1.065 is close to the equilibrium value of 1.075 at 25°C, suggesting that the kinetic isotope effects are small in sedimentary environments with a slow rate of sulfate reduction. Recently, Canfield *et al.* (2006) also reported a positive correlation between isotope fractionation and sulfate reduction rate. Detmers *et al.* (2001) and Shen and Buick (2004), however, found no evidence for such correlation in pure cultures or in natural populations.
(2) Within an organism's growth range, specific rates of bacterial sulfate reduction increase with increasing temperature – by two orders of magnitude from about 0° to 40°C – and by the availability of oxidizable organic substrates (i.e., digestible foods) (Ohmoto and Goldhaber, 1997). Experimental study by Canfield *et al.* (2006), however, showed that the relationship is nonlinear: the largest fractionation occurred at low and high temperatures, and the lowest fractionation in the intermediate temperature range.
(3) Fractionation tends to be lower when H_2 is the electron donor, particularly at low specific rates of sulfate reduction.
(4) Fractionation is influenced by the concentration of sulfate. In studies of pure cultures and natural populations, and with abundant sulfate (> 1 millimolar), fractionation has been measured in the range of 5–46‰ (Shen and Buick, 2004), largely independent of absolute sulfate abundance. At low sulfate concentrations, the rate at which sulfate enters the cell is reduced, thereby reducing also the rate of sulfate reduction, and fractionations become very small (≤ 4‰) when sulfate concentration drops below about 1 mM. According to Habicht *et al.* (2002), the transition between high and low fractionation is sharply defined at around 200 μM sulfate concentration.

The generally accepted isotopic signatures of BSR are large spreads in $\delta^{34}S$ values of sulfides (dominantly pyrite) with abundant negative values, and large isotopic offsets between coeval sulfate and sulfide. Fractionation resulting from BSR can be up to −65‰ (i.e., the H_2S or the metal sulfides that originate from BSR could be 65‰ lighter than their parent sulfate) because of the formation of intermediate compounds, such as thiosulfate or polysulfides, as well as disproportionation of these compounds (Jorgensen *et al.*, 1990).

11.7.2 *Thermochemical sulfate reduction (TSR)*

There exists reliable thermometric data indicating that many sedimentary sulfide deposits formed at temperatures that might have been above the tolerance limits of sulfate-reducing bacteria. In such cases, nonbacterial, chemical reduction of sulfate by methane or associated organic matter might have provided H_2S required for the precipitation of sulfides (Barton, 1967).

The kinetic sulfur isotope fractionation by TSR, which is much less compared to that by BSR, decreases with increasing temperature (e.g., ~20‰ at 100°C, ~15‰ at 150°C, ~10‰ at 200°C). On the basis of available experimental data and theoretical considerations, Kiyosu and Krouse (1990) proposed the following equation to describe the temperature dependence of TSR:

$$1000\ (\alpha_{\text{sulfate–sulfide}} - 1) = 3.32\ (10^6/T^2) - 4.91 \qquad (11.49)$$

where $\alpha_{\text{sulfate–sulfide}}$ is the fractionation factor in per mil and T is the temperature in Kelvin. In some natural systems, $\delta^{34}S$ values of sulfides and source sulfates are consistent with those obtained by using equation (11.49) (see, for instance, Machel *et al.*, 1995), but in some deep sour gas reservoirs the parent sulfate and the associated sulfides have nearly the same $\delta^{34}S$ values. For example, the very positive $\delta^{34}S$ values of H_2S in many natural gas fields (about +20‰ or more; Thode and Monster, 1965), approaching that of the source evaporite sulfate, probably reflect the almost complete reduction of sulfate by organic matter at less than 200°C in a system closed to sulfate but open to H_2S (Ohmoto 1986; Krouse *et al.*, 1988).

The lower temperature limit of TSR is not well defined. Available experimental data suggest that nonbacterial reduction of sulfates takes place at sufficiently high rates in the laboratory at temperatures above about 175°C, although it may occur at temperatures as low as about 100°C; as has been interpreted, for example, for the Pine Point (Canada) lead–zinc deposit (Powell and Macqueen 1984). According to Machel *et al.* (1995), TSR is a late diagenetic process, which generally requires temperatures greater than 100°C, anoxic conditions, and the presence of hydrocarbons.

11.7.3 *Sulfur isotopic composition of seawater sulfate through geologic time*

Evaluation of the sulfur isotope data for marine sedimentary sulfides requires knowledge of the isotopic composition of the source sulfate, the dissolved sulfate in coeval seawater. The isotopic fractionation during inorganic precipitation of minerals from seawater is negligible, in the order of 0 to +2.4‰ only. This is the reason why the isotopic compositions of ancient evaporite (gypsum and anhydrite) deposits have been used to estimate the $\delta^{34}S$ values of coeval seawater sulfate through geologic time. Claypool *et al.* (1980) were the first to present a compilation of marine evaporite data spanning the Phanerozoic and Late Precambrian (Fig. 11.7). According to their estimate, the $\delta^{34}S$ value of ancient seawater sulfate fluctuated between approximately +10 and +35‰ and averaged around +17‰ over the past 1000 Myr. The main features of the sulfur isotope age curve are: a pronounced maximum ($\delta^{34}S \approx +30$‰) at the end of the Proterozoic; gradual decrease to a Permian minimum ($\delta^{34}S \approx +10$‰), with a minor excursion during the Devonian ($\delta^{34}S \approx +25$‰); and then an increase towards the value for modern oceanic sulfate ($\delta^{34}S \approx +21$‰). This compilation has been refined by addition of new evaporite

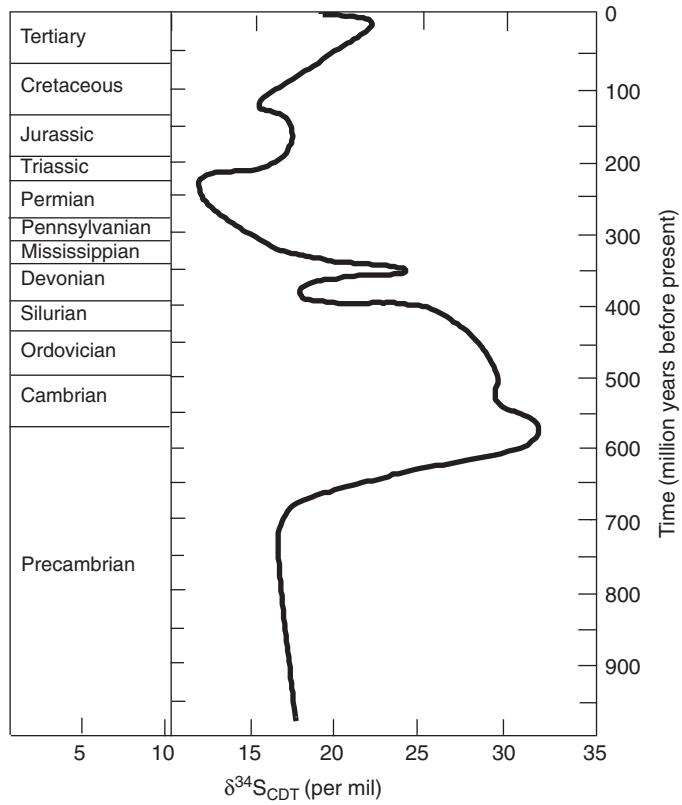

Fig. 11.7 Best estimate of secular variation of $\delta^{34}S_{CDT}$ of seawater based on evaporite derived sulfate–sulfur. The Proterozoic portion of the curve is based on very few data points, and there is a lack of data for the Archean because of the paucity of evaporite deposits. (After Bottrell and Newton, 2006, modified from Claypool *et al.*, 1980.)

data (e.g., Strauss, 1997, 1999), but the overall picture remains essentially the same. The secular variation in $\delta^{34}S$ has been attributed to fluctuations in the rate of production and burial of ^{34}S-depleted sedimentary sulfides, and the consequent enrichment of seawater sulfate in ^{34}S to maintain the overall mass balance of sulfur isotopes.

The evaporite record, however, suffers from some fundamental limitations. The rock successions do not contain a continuous record of evaporite deposits, either due to non-deposition or lack of preservation, and without fossils for biostratigraphic correlation the known evaporite deposits are not always well constrained in geologic age. An alternative approach followed recently by many workers (e.g., Kampschulte *et al.*, 2001; Lyons *et al.*, 2004; Kah *et al.*, 2004) uses trace sulfates (ranging in concentration from several hundred to a few thousand ppm) in biogenic limestones as a proxy for the seawater sulfate. Precipitation of calcium sulfate during precipitation of evaporites is associated with a very small isotopic fractionation ($\delta^{34}S = 0$ to +2‰; Holser and Kaplan, 1966), and the sulfate incorporation into the carbonate mineral lattice is not associated with any isotopic fractionation (Kampschulte *et al.*, 2001). Moreover, the carbonate-associated sulfate (CAS) gets excluded from the lattice of carbonate minerals during recrystallization without any significant sulfur isotope effect. Thus, CAS preserves the sulfur isotopic composition of contemporaneous seawater sulfate. CAS offers a better time resolution of the isotopic data because carbonate sequences provide a more continuous record than marine evaporite sulfate deposits and they also generally contain fossils that allow chronostratigraphic correlation. The CAS approach, for example, has resulted in a more reliable reconstruction of the isotopic composition of seawater sulfate during the Proterozoic for which evaporite sulfate data points are very limited (Bottrell and Newton, 2006).

11.7.4 *Open versus closed sedimentary systems with respect to sulfate and sulfide*

We adopt here the definitions of *open* and *closed* systems with respect to sulfate (SO_4^{2-}) and sulfide (H_2S) as discussed by Ohmoto and Goldhaber (1997). A sedimentary system can be considered open with respect to H_2S produced by reduction of SO_4^{2-} if the H_2S escapes to the overlying oxygenated sediments and water column or is fixed as iron sulfides and organic sulfur that, as a first order approximation, may be assumed to be nonreactive to SO_4^{2-}. In other words, in a system open to H_2S, the H_2S is removed from the system as soon as it is formed; if not, the system is closed with respect to H_2S. A system is considered open with respect to SO_4^{2-} when the supply rates of SO_4^{2-} are much faster than the rates of its reduction, irrespective of the absolute rate of sulfate reduction, so that the isotopic composition of SO_4^{2-} is maintained at a constant level for all practical purposes. Examples of open sulfate systems are a bioturbation zone (typically 0 to ~20 cm depth zone) in normal marine sediments, which is stirred by feeding activities of benthonic organisms, and the anoxic water body in euxinic basins. A system is considered closed with respect to SO_4^{2-} when the rate of sulfate reduction exceeds that of sulfate supply, so that the isotopic composition of the remaining sulfate changes as the reduction progresses and all sulfate may eventually be consumed within the system. Examples of closed sulfate systems are sedimentary sections beneath the bioturbation zone under oxic seawater and the sediments underlying the anoxic water column in euxinic basins.

In a system that is open to both SO_4^{2-} and H_2S, $\delta^{34}S_{SO_4}$ and $\delta^{34}S_{H_2S}$ values remain constant, despite variations in the sulfide content of the system, and so does the value of $\Delta_{SO_4-H_2S}$ (see equation 11.7). For example, assuming an average $\alpha_{SO_4-H_2S} = 1.025$ and $\delta^{34}S_{SO_4} = 20‰$ for seawater, bacterial isotopic fractionation would result in H_2S and precipitated pyrite having $\delta^{34}S \approx 5‰$. The relationship between $\delta^{34}S$ values of SO_4^{2-} and H_2S in a system that is closed to both and in which the two sulfur species are in equilibrium is shown in Fig. 11.8a. For a system closed to SO_4^{2-}, but open to H_2S, the fractionation can be described by the Rayleigh distillation model (equation 11.34) and is shown in Fig. 11.8b. Sulfides precipitated as a result of Rayleigh fractionation tend to be characterized by a large spread in $\delta^{34}S$ values, abundant negative values, and a progressive increase in $\delta^{34}S$ values toward the stratigraphic top in a sedimentary sequence (although the

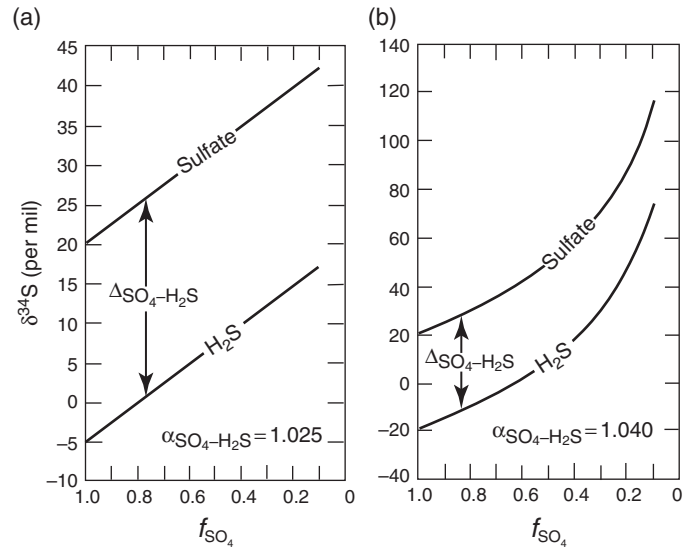

Fig. 11.8 Sulfur isotopic compositions of coexisting aqueous SO_4^{2-} and H_2S: (a) system closed to both SO_4^{2-} and H_2S, and in which the two sulfur species are in equilibrium; and (b) system closed to SO_4^{2-}, but open to H_2S (Rayleigh fractionation). f_{SO_4} denotes the atomic fraction of the initial SO_4^{2-} source remaining at a given instant of time. Note that in both cases, the SO_4^{2-} and H_2S are progressively enriched in ^{34}S relative to the starting sulfate composition as the reduction progresses toward completion, with a constant $\Delta_{SO_4-H_2S}$ in the case of (a) and decreasing $\Delta_{SO_4-H_2S}$ in the case of (b).

Box 11.3 Equations for sulfur isotope fractionation in selected sedimentary systems at constant temperature

(a) System open with respect to both SO_4^{2-} and H_2S

$\delta^{34}S_{SO_4}$ value remains the same as the initial value and $\delta^{34}S_{H_2S}$ attains a constant value at equilibrium given by (see equation. 11.10):

$$\delta^{34}S_{H_2S} = \frac{\delta^{34}S_{SO_4}^{initial} + 1000}{\alpha_{SO_4-H_2S}} - 1000 \quad (11.50)$$

(b) System closed with respect to both SO_4^{2-} and H_2S

As the fractionation progresses, values of both $\delta^{34}S_{SO_4}$ and $\delta^{34}S_{H_2S}$ change, which can be calculated using the following equations (Ohmoto and Goldhaber, 1997), but $\Delta_{SO_4-H_2S}$ remains constant at equilibrium:

$$\delta^{34}S_{H_2S} = \delta^{34}S_{SO_4}^{initial} - f_{SO_4}(1000 \ln \alpha_{SO_4-H_2S}) \quad (11.51)$$

$$\delta^{34}S_{SO_4} = \frac{\delta^{34}S_{SO_4}^{initial} - \delta^{34}S_{H_2S}\,(1 - f_{SO_4})}{f_{SO_4}} \quad (11.52)$$

(c) System closed with respect to SO_4^{2-} but open with respect to H_2S (Rayleigh fractionation; see Box 11.2)

As the fractionation progresses, values of both $\delta^{34}S_{SO_4}$ and $\delta^{34}S_{H_2S}$ change, which can be calculated using the following equations:

$$\delta^{34}S_{SO_4}^{remaining} = (\delta^{34}S_{SO_4}^{initial} + 1000) f_{SO_4}^{(1/\alpha_{SO_4-H_2S}-1)} - 1000 \quad (11.53)$$

$$\delta^{34}S_{H_2S} = (\delta^{34}S_{SO_4}^{remaining} + 1000)\,(1/\alpha_{SO_4-H_2S}) - 1000 \quad (11.54)$$

In the above equations, $\delta^{34}S_{SO_4}^{initial}$ represents the isotopic composition of the initial source sulfate, f_{SO_4} the atomic fraction of SO_4^{2-} remaining in the system at any particular extent of the system's evolution relative to the original amount, $\delta^{34}S_{SO_4}^{remaining}$ and $\delta^{34}S_{H_2S}$ the corresponding isotopic compositions for any particular value of f_{SO_4}, and $\alpha_{SO_4-H_2S}$ the fractionation factor between SO_4^{2-} and H_2S.

$\delta^{34}S$ value of the total sulfide mass would tend to be identical to the $\delta^{34}S$ value of the initial SO_4^{2-}). Equations to calculate $\delta^{34}S_{SO_4}$ and $\delta^{34}S_{H_2S}$ describing the relationships in the idealized systems mentioned above are given in Box 11.3. In natural sediments, however, there are no simple "open" or "closed" systems, and the interpretation of sulfur isotopic ratios is more complicated. Variable but typically negative $\delta^{34}S_{sulfide}$ values of sedimentary pyrites have generally been regarded as evidence of BSR (and Rayleigh fractionation), but this qualitative conclusion is insufficient to explain the observed variability in $\delta^{34}S_{sulfide}$ distribution in some individual stratigraphic units.

11.7.5 Sulfur isotope ratios of sulfides in marine sediments

A compilation of $\delta^{34}S$ values of sulfides in modern and ancient marine sediments over geologic time (Fig. 11.9) reveals several interesting features (Canfield and Teske, 1996; Habicht and Canfield, 2001a; Lyons *et al.*, 2004; Shen and Buick, 2004; Zahnle *et al.*, 2006):

(1) The $\delta^{34}S$ values of sulfides in modern and ancient marine sediments cover a wide range, from about −50‰ to about +40‰ (mostly to about +30‰).
(2) The sulfides of Archean age (> 2.5 Ga) are characterized by very low $\delta^{34}S$ values, within ±5‰ of the contemporaneous seawater sulfate (Habicht and Canfield, 1996, p. 342; Canfield *et al.*, 2000), but there is a sudden, marked increase at ~2.3–2.4 Ga, close to the beginning of the Paleoproterozoic.
(3) The next major increase in sulfur isotope fractionation occurs in the Neoproterozoic, at 0.7–0.8 Ga (Canfield, 2005). Phanerozoic sulfides are highly fractionated, the observed $\delta^{34}S$ values for the entire Phanerozoic ranging from about +40‰ to about −50‰. Modern sediments contain the most ^{34}S-depleted sulfides, with $\delta^{34}S$ values as low as −50‰ corresponding to a fractionation of about 70‰ relative to the present-day seawater sulfate ($\delta^{34}S$=+ 21‰). The 2.3–2.4 Ga and 0.7–0.8 Ga transitions in the sulfur

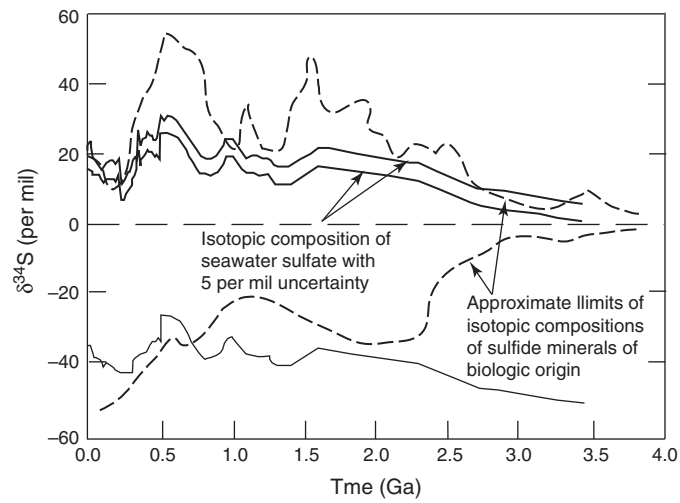

Fig. 11.9 The secular trends in the isotopic composition of seawater sulfate and sulfide minerals of likely biological origin over geological time. The band (double line) in the upper part of the figure represents the inferred isotopic composition of seawater sulfate (mostly anhydrite and gypsum), with 5‰ uncertainty, through geologic time. The single line in the lower part of the figure represents the isotopic composition of sulfate displaced by 55‰ to more ^{34}S-depleted values. Before 2.2 Ga the isotope composition of sulfate is determined mostly from barites, and constraints on the isotopic composition of seawater sulfate before 1.7 Ga are sparse. (Sources of data: Canfield, 1998; Canfield and Raiswell, 1999; Shen *et al.*, 2001.)

isotope record of sedimentary sulfides (Fig. 11.9) are broadly consistent with a two-step oxygenation of the Proterozoic atmosphere (see Chapter 13).

A combination of the secular variation in $\delta^{34}S$ of seawater sulfate Fig. 11.9 and the likely range of kinetic isotope effect (1.015–1.065) should result in a large range of fractionation (with mean $\delta^{34}S$ values in the range of approximately −50 to +15‰) in sedimentary sulfides produced by BSR. However, it appears that BSR cannot account for ^{34}S depletion (the difference between the isotopic composition of sulfate and sulfide) greater than about 46‰, the maximum ^{34}S depletion (the difference between the isotopic composition of the sulfate and sulfide) that has been observed in pure bacterial cultures and in natural populations from highly active microbial mats (Canfield and Teske, 1996; Habicht and Canfield, 1997). The large ^{34}S depletion found in some Phanerozoic sedimentary sulfides (up to 71‰; Canfield and Teske, 1996) is thought to have resulted from an initial fractionation by sulfate–reducing bacteria followed by one or more cycles of bacterially mediated oxidation of H_2S to intermediate sulfur species such as elemental sulfur (S^0), sulfite (SO_3^{2-}), and thiosulfate ($S_2O_3^{2-}$), and their disproportionation to ^{34}S-depleted SO_4^{2-} and H_2S (Jorgensen, 1990; Canfield and Teske, 1996; Habicht *et al.*, 1998). The *disproportionation reactions* (chemical reactions in which an element in one oxidation state in the reactants is converted into two or more oxidation states in the products) can be represented as follows:

$$S_2O_3^{2-} + H_2O \Rightarrow H_2S + SO_4^{2-} \quad (11.55)$$

$$4SO_3^{2-} + 2H^+ \Rightarrow H_2S + 3SO_4^{2-} \quad (11.56)$$

$$4S^o + 4H_2O \Rightarrow 3H_2S + SO_4^{2-} + 2H^+ \quad (11.57)$$

In bacterial cultures, the largest observed isotope fractionation has been found to be associated with the disproportionation of $S_2O_3^{2-}$–^{34}S depletion of 20–37‰ in H_2S and ^{34}S enrichment of 7–12‰ in sulfate (Habicht *et al*, 1998).

Sulfur isotope fractionation by BSR is reduced at low sulfate concentrations and high temperatures. Ohmoto and coworkers (e.g., Ohmoto and Felder, 1987; Kakegawa and Ohmoto, 1999) have argued that the very low $\delta^{34}S$ values of the Archean marine sulfides can be explained by high rates of bacterial sulfate reduction in a warmer ocean (temperature ~30° to ~50°C) that contained appreciable amounts of sulfate (> 1 mM kg^{-1} H_2O), with $\delta^{34}S_{SO_4}$ values of ~ +3‰. However, ^{34}S depletion observed in sulfides in modern natural microbial mats and in experimental runs – under conditions of abundant sulfate (up to 65 mM kg^{-1} H_2O), high rates of sulfate reduction (≥ 10 μmol cm^{-3} d^{-1}), and elevated temperatures (up to 85°C) – range from 13 to 28‰ (Habicht and Canfield, 1996; Canfield *et al.*, 2000), much higher than the ^{34}S depletion observed in Archean sedimentary sulfides. The very small sulfur isotope fractionation in Archean sedimentary sulfides could be the consequence of a nonbiogenic source of sulfur, if sulfur-reducing bacteria had not yet evolved, but sulfate-reducing bacteria were active in the ocean by at least about 3.47 Ga (Shen *et al.*, 2001). The favored interpretation is that BSR in Archean seawater occurred in an environment of low concentration of dissolved sulfate (< 1 mM compared to the present value of 28 mM) that mirrored a lack of oxidative chemical weathering of sulfides (mainly pyrite), the main source of dissolved SO_4^{2-} in seawater, because of an oxygen-deficient atmosphere. Canfield *et al.* (2000) calculated that the complete oxidation of 100 μm pyrite grains in soils (sedimentary pyrites are typically of this size or smaller) should occur with water containing > 1 μM O_2, which is the amount of dissolved O_2 that would be in equilibrium with 0.4% PAL (the *present atmospheric level*) at 25°C. Thus, the sulfur isotope record is consistent with very low atmospheric O_2 concentrations (< 0.4% PAL, as a rough estimate) before ~2.4 Ga. It is also consistent with a lack of sulfate–evaporite deposits in the Archean.

The jump in sulfur isotope fractionation at 2.4–2.3 Ga marked the rise in seawater sulfate concentration to > 1 mM, approximately coincident with the timing of the first stage of a rise in Earth's atmospheric oxygen, often referred to as the *Great Oxidation Event* (Holland, 2002). The fractionations during the interval between 2.4–2.3 Ga and 0.8–0.7 Ga are consistent with 40–45‰ as the upper limit of fractionation via BSR in an ocean containing > 1 mM dissolved sulfate. The dramatic increase in fractionation after ~0.8–0.7 Ga was probably caused by additional fractionations produced by disproportionation of sulfur-containing species (such as S^0, SO_3^{2-}, $S_2O_3^{2-}$) due to greater oxygen availability in the ocean–atmosphere system, leading to evolutionary development of nonphotosynthetic sulfide-oxidizing bacteria and enhanced biotic oxidation of sulfides to intermediate sulfur species (Canfield and Teske, 1996; Lyons *et al.*, 2004). According to Canfield and Teske (1996), atmospheric O_2 in excess of 5–18% PAL would have been high enough to substantially oxidize the surface seafloor in nearshore settings, thus accelerating the formation of intermediate sulfur compounds and the disproportionation process (Canfield, 2005). The two-step oxygenation of the Proterozoic atmosphere, corresponding to the two major transitions in the sulfur isotope record, is compatible with the $\delta^{13}C$ chemistratigraphy of sedimentary carbonates and organic matter (Des Marais *et al.*, 1992; Karhu and Holland, 1996; Kump and Arthur, 1999; Kah *et al.*, 2004). The evolution of the Earth's atmosphere and oceans will be discussed in more detail in Chapter 13.

11.8 Mass-independent fractionation (MIF) of sulfur isotopes

So far our discussion has been restricted to mass-dependent equilibrium and kinetic isotope fractionations of sulfur isotopes, fractionations that are governed primarily by the

relative mass differences between isotope species. For sulfur isotopes, this dependence is indicated by highly correlated linear arrays on plots of $\delta^{33}S$ versus $\delta^{36}S$ and $\delta^{36}S$ versus $\delta^{34}S$ for terrestrial sulfide samples younger than 2000 Ma ($\delta^{33}S \approx 0.515\ \delta^{34}S$; $\delta^{36}S \approx 1.91\ \delta^{34}S$; Hulston and Thode, 1965) (Fig. 11.10a). *Mass-independent fractionation* (MIF), on the other hand, is characterized by isotopic compositions that do not plot on the mass-dependent fractionation line (Fig. 11.10b). The strategy for distinguishing between mass-dependent and mass-independent fractionation is similar for other stable isotope systems, such as iron isotopes (Beard and Johnson, 2004).

Strong evidence for an anoxic atmosphere during the Archean is provided by the fact that MIF of sulfur isotopes has been reported in sediments of Archean and Early Proterozoic age (> 2.45 Ga) but not in younger sediments (Farquhar *et al.*, 2000; Farquhar and Wing, 2003; Mojzsis *et al.*, 2003; Papineau and Mojzsis, 2006). Farquhar *et al.* (2001) showed experimentally that MIF-S occurs via gas-phase photochemical reactions such as *photolysis* (see section 13.1) of SO_2 and SO in the stratosphere (see Fig. 13.2) by UV radiation in the 190–220 nm spectral region, the region of wavelengths at which UV radiation is strongly absorbed by ozone and oxygen. Thus, the penetration of such shortwave radiation deep into the atmosphere to cause photolysis of SO_2 could have happened only when the column abundances of ozone and oxygen in the Earth's atmosphere were much lower than at present. Using a one-dimensional photochemical model, Pavlov and Kasting (2002) showed that in an essentially anoxic atmosphere with O_2 concentrations $<10^{-5}$ PAL (i.e., < 2 ppmv), sulfur would be removed from the atmosphere in a variety of oxidation states (from –2 as in H_2S to +6 as in H_2SO_4), each with its own distinct isotopic signature, and incorporated into sediments. On the other hand, in an atmosphere with O_2 concentrations $\geq 10^{-5}$ PAL, any signature of atmospheric MIF-S would be lost because of the oxidation of sulfur-bearing species to H_2SO_4 and subsequent rehomogenization of the sulfur isotopes in the oceanic reservoir (e.g., by mixing with magmatic sulfur with $\Delta^{33}S = 0$ exhaled through submarine volcanism) before being transferred into sediments.

Figure 11.11 is a plot of $\Delta^{33}S$ as a function of age of sedimentary sulfide and sulfate minerals, where the quantity $\Delta^{33}S$ reflects the deviation of measured $\delta^{33}S$ and $\delta^{34}S$ from the $\delta^{34}S - \delta^{33}S$ mass-dependent fractionation array (see Fig. 11.10a), the mass-dependent reference value, and is calculated as (Farquhar and Wing, 2003):

$$\Delta^{33}S = \delta^{33}S - 1000\left(\left(1 + \frac{\delta^{34}S}{1000}\right)^{0.515} - 1\right) \tag{11.58}$$

The $\Delta^{33}S$ record divides the Earth's history into three stages that reflect fundamental changes in the Earth's atmosphere as well as in its sulfur cycle through time (Farquhar and Wing, 2003). Stage I, characterized by a large range of $\Delta^{33}S$ values, represents an anoxic atmosphere. A low-O_2 atmosphere, $<10^{-5}$ PAL according to modeling by Pavlov and Kasting (2002), is necessary for the production of nonzero $\Delta^{33}S$ values, because ozone shields UV radiation at high O_2 levels, inhibiting the photochemical reactions that produce mass-independent fractionation. Low O_2 levels are also necessary for the preservation of nonzero $\Delta^{33}S$ values during the transfer of both oxidized and reduced sulfur species to the surface (Pavlov and Kasting, 2002) and for the retention of the $\Delta^{33}S$ differences between them in surface environments (Farquhar *et al.*, 2000). Stage II is marked

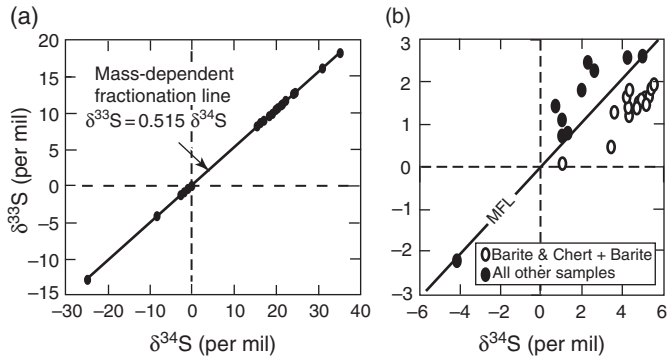

Fig. 11.10 Plot of $\delta^{33}S$ versus $\delta^{34}S$ for terrestrial sulfide (pyrite) and sulfate (barite) samples: (a) samples younger than 2000 Ma, which form a tightly constrained linear array, the mass dependent fraction line (MFL), defined by the relation $\delta^{33}S \approx 0.515\ \delta^{34}S$; and (b) samples older than 3000 Ma, which do not plot on the MFL and represent mass independent fractionation (MIF). (Sources of data: Farquhar *et al.*, 2000; Mojzsis *et al.*, 2003; Hu *et al.*, 2003. After Farquhar *et al.*, 2000, Fig. 3(B), p. 758; Farquhar *et al.*, 2001, Figure 1, p. 32830.)

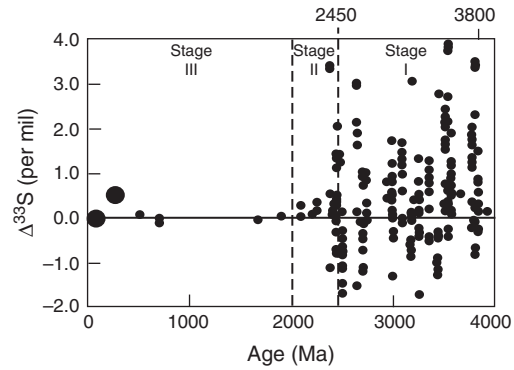

Fig. 11.11 Plot of $\Delta^{33}S$ versus age for terrestrial sulfide (pyrite) and sulfate (barite) samples. The large filled circle represents hundreds of analyses of samples younger than 2.0 Ga. The change from Stage I to Stage II is attributed to a change in the Earth's atmospheric chemistry. Photolysis reactions involving SO_2 and SO in the Earth's early atmosphere, coupled with an efficient transfer of the signature to the Earth's surface, produced this record. The smaller Stage II record may reflect the onset of oxidative weathering or it may reflect stabilization of atmospheric oxygen to intermediate levels (10^{-5}–10^{-2} PAL). (Sources of data: Farquhar *et al.*, 2000, 2001; Heymann *et al.*, 1998; Mojzsis *et al.*, 2003. After Farquhar and Wing, 2003 Figure 1, p. 3.)

by a smaller range of $\Delta^{33}S$ variability (–0.2 to +0.5‰) and is interpreted to indicate the beginning of a dramatic increase in the concentration of free O_2 in the atmosphere around 2.45 Ga. Stage III is characterized by near-zero $\Delta^{33}S$ values (generally much smaller than ±0.2‰) and represents a record of dominantly mass-dependent fractionation over the past 2 Gyr under an oxic atmosphere with increased concentration of atmospheric O_2, probably to > 1% PAL. The oxidation of Fe^{2+} in paleosols and the lack of detrital uraninite in sediments are consistent with atmospheric O_2 concentration of $\geq 10^{-2}$ PAL sometime after 2.3 Ga (Holland, 1984,1994) (see Chapter 13). Syngenetic pyrite from organic-rich shales of the 2.32 Ga Rooihoogte and Timeball Hill formations, South Africa, show no evidence of MIF-S, and large MIF-S signals do not reappear thereafter, indicating that the rise of atmospheric oxygen had occurred by 2.32 Ga (Bekker *et al.*, 2004). Thus the MIF-S record points to a significant rise in atmospheric O_2 between 2.45 and 2.32 Ga, and the transition to an oxygen-rich terrestrial atmosphere according to Farquhar and Wing (2003) was complete by 2 Ga.

A different interpretation was offered by Zahnle *et al.* (2006), who attributed the loss of MIF-S signature in sediments to a collapse of the atmospheric methane in the late Archean, not to a rise in the atmospheric oxygen. A key player in the MIF-S story was elemental sulfur (S_8), a major product of dissociation of SO_2 gas by solar UV radiation in an anoxic atmosphere. The insoluble S_8 particles rained out of the atmosphere, were incorporated in sediments, and preserved the MIF-S signal. Conditions conducive to the formation of S_8 are a source of sulfur (such as volcanic eruptions, at least as large as the volcanic SO_2 source today), an anoxic troposphere, and sufficient amount of a reduced gas (such as CH_4). According to Zahnle *et al.* (2006), a decrease in the atmospheric CH_4 from hundreds of ppmv to below 10 ppmv would eliminate the MIF-S signal. The methane collapse was driven by the increasing importance of dissolved sulfate in the oceans and the increasing competitive advantage of sulfate reducers over methanogens. This scenario would be consistent with the onset of low-latitude glaciation ("Snowball Earth") around ~2.4 Ga. The rise of oxygen to geologically detectable levels occurred after the loss of MIF-S, and was facilitated by generally low levels of atmospheric CH_4 characteristic of the ice ages.

11.9 Iron isotopes: geochemical applications

Transition metals are potentially well suited to be used as proxies for assessing the redox state of ancient oceans because their chemical transformations and speciation are closely coupled to the availability of oxygen in the environment. A promising element in this connection is iron because the oxidation of Fe(II) to Fe(III) in aqueous solutions is typically accompanied by significant fractionation of iron isotopes. A number of laboratories around the world are now investigating the application of iron isotopes to a variety of topics: the study of human blood, pathways of Fe cycling in modern oceans, redox cycling in ancient Earth, and differentiation of the Solar System. Our current understanding of the iron isotope geochemistry has been summarized in a number of recent review papers such as Anbar (2004), Beard and Johnson (2004), Anbar and Rouxel (2007), and Johnson *et al.* (2008a,b).

11.9.1 *Fractionation of iron isotopes*

Iron, the fourth most abundant element in the Earth's crust, has four naturally occurring stable isotopes: ^{54}Fe (5.84%), ^{56}Fe (91.76%), ^{57}Fe (2.12%), and ^{58}Fe (0.28%). The different behavior of Fe(II) compared to Fe(III), and the significant isotopic fractionations (1‰ or more in $^{56}Fe/^{54}Fe$ ratio) that are associated with redox conditions, suggest that Fe isotopes should be useful for tracing the geochemical cycling of Fe.

Iron isotope data are typically reported as $\delta^{56}Fe$:

$$\delta^{56}\text{Fe (per mil)} = \left(\frac{\left(^{56}\text{Fe}/^{54}\text{Fe}\right)_{\text{sample}}}{\left(^{56}\text{Fe}/^{54}\text{Fe}\right)_{\text{Ign Rocks}}} - 1 \right) 10^3 \tag{11.59}$$

which is of the same form as equation (11.3). $(^{56}Fe/^{54}Fe)_{\text{Ign Rocks}}$ is defined by the average of a wide spectrum of terrestrial igneous rocks that have a near-constant Fe-isotopic composition of $\delta^{56}Fe = 0.00 \pm 0.05$ (1σ)‰, irrespective of age, location, composition, and tectonic setting (Beard *et al.*, 2003). A standard commonly used for facilitating interlaboratory comparison of data is the Fe-metal isotope standard IRMM-014; the two reference frames for $\delta^{56}Fe$ are related as:

$$\delta^{56}\text{Fe}_{\text{Ign Rocks}} = \delta^{56}\text{Fe}_{\text{IRMM-014}} - 0.09‰ \tag{11.60}$$

Between two Fe-bearing species, A and B, the mass-dependent isotopic fractionation factor (α_{A-B}) and the isotopic fractionation ($\Delta^{56}Fe_{A-B}$), which may reflect equilibrium or kinetic isotope effects or a combination of the two, are related the same way as other stable isotopes:

$$\Delta^{56}\text{Fe}_{\text{A–B}} = 1000 \ln \alpha_{\text{A–B}} \approx \delta^{56}\text{Fe}_{\text{A}} - \delta^{56}\text{Fe}_{\text{B}} \tag{11.61}$$

Natural mass-dependent variations of $\delta^{56}Fe$ values, whether generated by abiotic or biotic processes, are small and cover a range of only ~4‰ (from ~ +1.0 to –3.0‰; Fig. 11.12), an order of magnitude smaller than the variations observed for $\delta^{34}S$. Fortunately, modern multiple collector inductively coupled plasma mass spectrometers (MC–ICP–MS) are capable of routinely measuring $\delta^{56}Fe$ values to a reported external precision of ±0.1‰ (2σ) in samples weighing < 1 μg, which is adequate to examine iron isotope fractionation in nature (Anbar, 2004, p. 225).

The most important controls on iron isotope fractionations in natural, low-temperature systems are the oxidation state of the species and the strength of their bonds. Molecular vibration theory predicts that iron isotopes may be fractionated during equilibrium (reversible) and disequilibrium (irreversible) abiotic

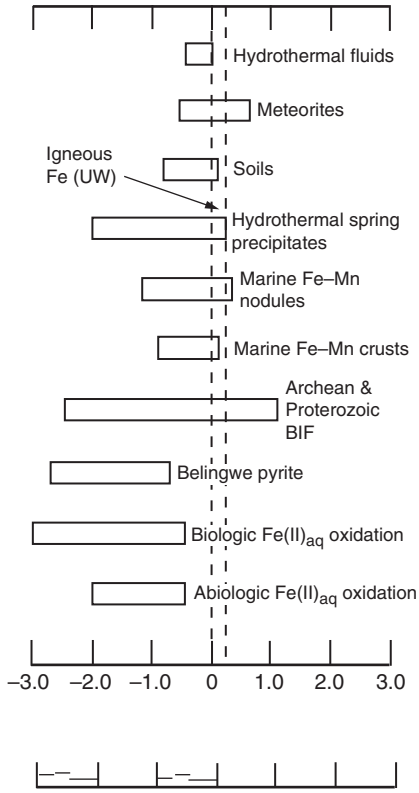

Fig. 11.12 δ^{56}Fe variations in some natural materials and experimental studies of Fe^{2+}_{aq} oxidation. The box for each category represents the maximum observed range. For California coastal samples, the Fe^{3+} / Fe_{total} ratio exceeds 0.3, reflecting an important influence by Fe^{3+}-reducing bacteria. (Sources of data: Archer and Vance (2006); compilations by Johnson *et al.* (2003), Anbar (2004), and Johnson and Beard (2006).)

reactions between minerals and fluids due to the relative stability of the heavier isotopes in more strongly bonded minerals and aqueous species. Under equilibrium conditions, aqueous Fe^{3+} or compounds that are composed entirely of Fe(III) (e.g., ferrihydride, represented in this discussion as $Fe(OH)_{3(s)}$, which eventually crystallizes to hematite, Fe_2O_3, without any further Fe isotope fractionation) have higher δ^{56}Fe values than those of mixed Fe^{3+}–Fe^{2+} oxidation state (e.g., magnetite, $Fe^{2+}O.Fe^{3+}_2O_3$), and aqueous species or minerals in which the iron is entirely Fe^{2+} (e.g., siderite, $FeCO_3$) tend to have the lowest δ^{56}Fe values. Exceptions to these general trends in equilibrium fractionation include aqueous species or minerals with covalently bonded Fe, such as pyrite, which has relatively high δ^{56}Fe values. As is the case with isotopes of other bioreactive elements (such as carbon, nitrogen, sulfur, and oxygen), Fe isotopes can be fractionated by microbes during both dissimilatory Fe(III) reduction (DIR), in which Fe(III) acts as an electron acceptor for respiration, and assimilatory iron metabolism, which involves uptake and incorporation of iron into biomolecules. Both processes result in depletion of the product in ^{56}Fe relative to ^{54}Fe.

Iron isotope variations observed in some natural materials and determined experimentally are shown in Fig. 11.12. Most of the Fe in the crust, including most igneous rocks as well as their alteration and weathering products, have a δ^{56}Fe value near zero (Johnson *et al.*, 2004b). So, measured nonzero δ^{56}Fe values for minerals and rocks have been produced by interaction with Fe-bearing fluids such as the hydrothermal fluids vented at mid-oceanic ridges. Modern MOR fluids have δ^{56}Fe values between –0.8‰ and –0.1‰, but the values were probably close to zero during the Archean because of higher heat flow (Johnson *et al.*, 2008a).

As summarized by Beard and Johnson (2004) and Johnson and Beard, (2006), experimental investigations have shown that the maximum fractionation between $Fe(OH)_{3(s)}$, the initial Fe^{3+}-precipitate formed by the two-step abiotic reaction, $Fe^{2+}_{aq} \Rightarrow Fe^{3+}_{aq} \Rightarrow Fe(OH)_{3(s)}$, and Fe^{2+}_{aq} (i.e., $\Delta_{Fe(OH)3(s)-Fe^{2+}_{aq}}$) is +3.0‰ at room temperature (i.e., $\alpha_{Fe(III)-Fe(II)}$ ~1.0030), reflecting a Fe^{3+}_{aq}–Fe^{2+}_{aq} fractionation of +2.9‰ and a very small $Fe(OH)_{3(s)}$–Fe^{3+}_{aq} fractionation of +0.1‰. The equilibrium $Fe(OH)_{3(s)}$–Fe^{3+}_{aq} fractionation is very small because the reaction does not involve a change in the oxidation state or coordination of Fe. The $Fe(OH)_{3(s)}$–Fe^{2+}_{aq} fractionation observed in nature is much less, generally between ~ +0.9 to +1.6‰, representing the sum of an equilibrium fractionation of +2.9‰ and a kinetic fractionation of –1.3‰ to –2.0‰ upon precipitation depending on precipitation kinetics. Thus, partial oxidation would produce ferric oxide/hydroxide precipitates that have positive δ^{56}Fe values, controlled by the net $Fe(OH)_{3(s)}$–Fe^{2+}_{aq} fractionation factor and the extent of reaction, whereas complete oxidation would produce no net change in the δ^{56}Fe value relative to that of Fe^{2+}_{aq}.

11.9.2 Abiotic versus biotic precipitation of Fe minerals in banded iron formations

Significant variations in Fe-isotope compositions of rocks and minerals appear to be restricted to chemically precipitated sediments, such as the Precambrian banded iron formations (BIFs; see Box 13.3). The Fe-isotope ratios in BIFs span almost the entire range yet observed on Earth because some of the largest Fe-isotope fractionations occur between Fe^{2+} and Fe^{3+} species involved in the precipitation of iron oxide and carbonate minerals in BIFs. The precipitation of hematite (Fe_2O_3) involves hydrothermal transport of dissolved Fe^{2+}, oxidation of Fe^{2+}_{aq} to Fe^{3+}_{aq}, and subsequent precipitation of Fe^{3+}_{aq} as $Fe(OH)_{3(s)}/Fe_2O_3$. The formation of magnetite (Fe_3O_4) and siderite ($FeCO_3$) requires reduction of Fe^{3+}_{aq} to Fe^{2+}_{aq}. Both the oxidation of Fe^{2+}_{aq} and the reduction of Fe^{3+}_{aq} can occur by abiotic or biotic processes (see Box 13.3).

Based on the hypothesis that Fe isotope fractionation by bacterially catalyzed kinetic processes would produce much larger effects compared to inorganic fractionation, particularly at

equilibrium, much of the initial research on Fe isotopes was prompted by the expectation that Fe-isotope compositions of Fe-bearing minerals could be used to differentiate between biotic and abiotic precipitation of $Fe(OH)_{3(s)}/Fe_2O_3$. So far, this approach has not met with conclusive results because the overall $Fe(OH)_{3(s)}/Fe_2O_3$–Fe^{2+}_{aq} fractionation, as determined by experiments (Bullen *et al.*, 2001; Croal *et al.*, 2004; Balci *et al.*, 2006; Staton *et al.*, 2006), appears to be similar regardless of the oxidative pathway involved. Thus, Fe isotopes, by themselves, do not appear to provide a clear discrimination between biotic and abiotic pathways that involve oxidation.

Detailed experimental studies indicate that bacterial iron reduction (BIR) produce low $\delta^{56}Fe$ values, $\Delta^{56}Fe_{Fe^{2+}_{aq}-Fe(OH)_{3(s)}} = -3.0‰$, whereas $\Delta^{56}Fe_{Fe_3O_{4(s)}-Fe^{2+}_{aq}} = +1.3‰$ and $\Delta^{56}Fe_{FeCO_{3(s)}-Fe^{2+}_{aq}} = -0.5‰$ (Johnson *et al.*, 2005, 2008b). Thus, negative $\delta^{56}Fe$ values of magnetite or siderite probably are a signature of biotic reduction of $Fe(OH)_{3(s)}/Fe_2O_3$ to Fe^{2+}_{aq}. A combination of low $\delta^{56}Fe$ values and covariation of $\delta^{56}Fe$ and $\delta^{34}S$, as has been documented for the sedimentary pyrite from the Belingwe greenstone belt, Zimbabwe (2.7 Ga), would provide strong evidence in favor of microbial Fe(III) reduction. This is because such covariation is most readily explained in terms of coupled Fe(III) and SO_4^{2-} reduction during microbial organic matter degradation, as occurs in modern anoxic sediments (Archer and Vance, 2006).

11.10 Summary

1. Some of the important applications of stable isotope geochemistry to natural geochemical systems include: geothermometry; evaluation of the sources of the stable isotopes in minerals, rocks, and fluids; recognition of bacterially mediated reactions in oxidation–reduction reactions, and evolution of the crust–ocean–atmosphere system through geologic time.
2. Stable isotope ratios of samples are reported as δ values, in per mil (‰), relative to appropriate reference standards: For example, $\delta^{18}O_{sample}$ is defined as:

$$\delta^{18}O_{sample}(\text{per mil}) = \frac{\left(R_{sample} - R_{std}\right)}{R_{std}} \times 10^3$$

where R_{sample} is the atomic ratio of the heavy to the light isotope in the sample (i.e., $^{18}O/^{16}O$), and R_{std} is the corresponding ratio in the reference standard.
3. The fractionation factor (α_{A-B}), the degree of isotopic fractionation between two coexisting phases A and B (Δ_{A-B}) in isotopic equilibrium, is defined as $\alpha_{A-B} = R_A/R_B$, and can be calculated from the equation

$$\alpha_{A-B} = \frac{R_A}{R_B} = \frac{\delta_A + 1000}{\delta_B + 1000}$$

or from the approximate relationship

$$1000 \ln \alpha_{A-B} \approx \delta_A - \delta_B = \Delta_{A-B}$$

if values of both Δ and δ_i are about ±10‰ or less. Between coexisting molecules the heavier isotope is preferentially partitioned into the one in which it can form stronger bonds.
4. Effects of isotopic fractionation are generally evaluated as: (i) equilibrium isotopic effects, produced by equilibrium isotope exchange reactions, which are independent of the pathways or mechanisms involved in the achievement of equilibrium; and (ii) kinetic isotopic effects, produced by unidirectional processes or unequilibrated chemical reactions (e.g., bacterially mediated reduction of SO_4^{2-} to H_2S), which depend on reaction mechanisms and possible intermediate products.
5. Stable isotope geothermometry is based on the variation of isotopic fractionation as a function of temperature; the effect of pressure is negligible in most systems, especially at < 10 kbar.
6. The progress of isotopic fractionation with time in a system depends on whether the system is closed or open to the parent and product species under consideration. For example, isotopic fractionation in a system such as water vapor (wv)–rainwater (rw), which is closed to the parent (wv) but open to the product species (rw), can be modeled by the Rayleigh distillation equation:

$$R = R_0 f^{(\alpha-1)}$$

7. The sulfate reduction of SO_4^{2-} to H_2S is either catalyzed by anaerobic, sulfate-reducing bacteria at relatively low temperatures (bacterial sulfate reduction, BSR), or it occurs at relatively elevated temperatures without the involvement of bacteria (thermochemical sulfate reduction, TSR). In either case, the product H_2S becomes enriched in ^{32}S relative to SO_4^{2-}.
8. The available record of $\delta^{34}S$ values of sulfides over geologic time appears to broadly correlate with a two-step oxygenation of the Proterozoic atmosphere at ~2.2–2.3 Ga and ~0.7–0.8 Ga.
9. Strong evidence for an anoxic atmosphere during the Archean is provided by the fact that mass-independent fractionation (MIF) of sulfur isotopes has been reported in sediments of Archean and Early Proterozoic age (> 2.3 Ga) but not in younger sediments.
10. Fe isotopes do not seem to provide a clear discrimination between biotic and abiotic pathways involving oxidation for the precipitation ferric hydroxides and oxides in banded iron formations (BIFs). Negative values of $\delta^{56}Fe$ for magnetite and siderite, on the other hand, appear to indicate biologic iron reduction (BIR).

11.11 Recapitulation

Terms and concepts

Assimilatory sulfate reduction
Anoxic atmosphere
Bacterial sulfate reduction (BSR)
Delta notation
Disproportionation reaction
Dissimilatory sulfate reduction
Great oxidation event
Isotope geothermometry
Isotopic effects (equilibrium and kinetic)
Isotopic fractionation (mass-dependent and mass-independent)
Isotopic fractionation factor
Kaolinite line
Meteoric water line (global and local)
Open and closed systems
Oxic atmosphere
Rayleigh distillation equation
SMOW
Thermochemical sulfate reduction (TSR)

Computation techniques

- Calculation of fractionation factor from δ values, and of $\delta_{product}$ from δ_{parent}, using fractionation factor.
- Calculations pertaining to isotopic stable isotope geothermometry (oxygen and sulfur).
- Calculations for fractionations in open and closed systems, including calculations using the Rayleigh distillation equation.

11.12 Questions

1. Hydrogen has two stable isotopes and oxygen has three. List the combinations for isotopically distinct water molecules, along with their masses.
2. The relative atomic abundance of oxygen and carbon isotopes are:

   ^{16}O: ^{17}O: ^{18}O = 99.759: 0.0374: 0.2039; and ^{12}C: ^{13}C = 98.9:1.1

   Calculate the relative abundances of (i) masses 44.0, 45.0 and 46.0 in CO_2, and (ii) masses 28.0, 29.0, and 30.0 in CO.
3. Calculate the $\delta^{13}C$ value of $CaCO_3$ precipitated in equilibrium with atmospheric CO_2 gas at 20°C, given that $\alpha_{CaCO_3-CO_2} = 1.01017$ and $\delta^{13}C_{CO_2} = -7.0‰$. What would be the $\delta^{13}C$ value of calcite precipitated at 20°C in isotopic equilibrium with atmospheric CO_2 if the $\delta^{13}C$ value of atmospheric CO_2 decreases to −12‰ due to increased burning of fossil fuels?
4. Consider a hypothetical sediment composed of 15 mol% of detrital quartz ($\delta^{18}O$ = +12‰) and 85 mol% marine calcite ($\delta^{18}O$ = + 28‰). Determine the oxygen isotopic composition of each mineral after metamorphic equilibration in a closed system at 500°C. $\alpha_{SiO_2-CaCO_3} = 1.01017$ at 500°C.
5. An air mass whose initial δD value is −71.4‰ at 25°C starts to condense into rain. Plot graphs showing the progressive change in the δD value of water vapor and the δD value of rainwater in equilibrium with that water vapor at 25°C. Assume $\alpha_{rainwater-water\ vapor} = 1.074$.
6. The fractionation of oxygen isotopes for the muscovite (mus)–water system as a function of temperature in the 500–800°C range can be described as (Bottinga and Javoy, 1973, p. 257):

   $$1000 \ln \alpha_{musc-water} = 1.90\ (10^6/T^2) - 3.10$$

   What is the $\delta^{18}O$ value of muscovite in equilibrium with water having $\delta^{18}O$ = −9‰ at 500°C?
7. A mineralized quartz vein contains rutile (rut) in equilibrium with quartz. Derive a quartz–rutile geothermometry equation and calculate the quartz–rutile equilibration temperature if $\delta^{18}O_{qz} - \delta^{18}O_{rut} = -4.60$ per mil. Equations describing the variation of mineral–water fractionation factors with temperature are (Friedman and O'Neil, 1977):

   $$1000 \ln \alpha_{qz\text{-}water} = 2.51\ (10^6/T^2) - 1.46\ (500–750°C)$$

   $$1000 \ln \alpha_{rut\text{-}water} = 4.10\ (10^6/T^2) + 1.46\ (575–775°C)$$

8. Plot graphs showing the variaton of $\delta_{mineral-water}$ as a function of temperature (t = 0 to 225°C) for calcite, quartz, and phosphate (calcite–water data relative to PDB standard; quartz–water and phosphate–water data relative to SMOW standard):

   (a) calcite–water: $t\ (°C) = 16.9 - 4.2\ (\delta_{calcite} - \delta_{water}) + 0.13\ (\delta_{calcite} - \delta_{water})^2$

   (b) quartz–water: $t\ (°C) = 169 - 4.1\ \{(\delta_{quartz} - \delta_{water}) + 0.5\}$

   (c) phosphate–water: $t\ (°C) = 111.4 - 4.3\ \{(\delta_{phosphate} - \delta_{water}) + 0.5\}$

   Comment on (i) the temperature dependence of the fractionation for all the three minerals, and (ii) the suitability of these mineral pairs as paleothermometers.
9. Given below are $\delta^{18}O$ and δD values of rainwater and snowmelt samples collected over a period of time at a certain locality in western USA. Plot the data and determine the linear regression equation for the local meteoric water line. How does it compare with the global meteoric water line of Craig (1961)?

δ18O ‰	δD ‰	δ18O ‰	δD ‰	δ18O ‰	δD ‰	δ18O ‰	δD ‰
–8.4	–55	–5.57	–23	–5.7	–21	–18.1	–120
–6.8	–44	–5.7	–21.5	–7.7	–43	–21.75	–163
–8.3	–55	–7.75	–42.5	–5.5	–25	–16.05	–116
–7.9	–52	–5.5	–25	–15.8	–111	–19.7	–128
–7.7	–51	–11.7	–78	–23.2	–151	–18.8	–137
–8.2	–56	–5.6	–23	–22.95	–182.3	–17.6	–129

10. Using the equations for $1000 \ln \alpha_{\text{quartz–H}_2\text{O}}$ and $1000 \ln \alpha_{\text{magnetite–H}_2\text{O}}$ given in Table 11.2, construct a calibration curve for $1000 \ln \alpha_{\text{quartz–magnetite}}$ as a function of temperature (in Kelvin) in the range $10^6/T^2=0$ to $10^6/T^2=6$ (x coordinate). What is the isotopic equilibrium temperature corresponding to $1000 \ln \alpha_{\text{quartz–magnetite}}=18.213$?
11. Calculate w/r ratios as a function of assumed δ^{18}O values for an altered igneous body, $\delta^{18}O^f_{\text{rock}}$, at different equilibraton temperatures (400°C, 500°C, and 600°C), and for "closed" and "open" system models of Taylor (1977). Assume that, at equilibrium, $\delta^{18}O^f_{\text{rock}}$ is equal to the δ^{18}O value of plagioclase (An_{30}) in the rock, and use the plagioclase (An_{30})–water geothermometer of O'Neil and Taylor (1967) to calculate $\Delta^{18}O_{\text{plag–water}}$: $\delta^{18}O^i_{\text{rock}}=+6.5‰$ and $\delta^{18}O^i_{\text{water}}=-14‰$. Show your results on a binary diagram, with x axis$=w/r$ ratios (atom% oxygen) and y axis$=\delta^{18}O^f_{\text{rock}}$. What generalized conclusions can you infer from your results?
12. The δ^{34}S value of the present-day seawater sulfate is 21‰. Calculate the value of $\alpha_{SO_4-H_2S}$ that would produce pyrite with a δ^{34}S value of –50‰ by sulfate reduction, assuming the system to be open with respect to both SO_4^{2-} and H_2S? What are the factors that determine the δ^{34}S values of marine sedimentary pyrites? What are the possible causes for the observation that the δ^{34}S value of pyrites in Archean marine sediments is only about –5‰?
13. Coexisting sphalerite (ZnS)–galena (PbS) pairs in a lead–zinc sulfide deposit in Providencia, Mexico, have δ^{34}S values (per mil) as listed below (Rye, 1974):

Sample number	δ^{34}S (galena)	δ^{34}S (sphalerite)
60-H-67	–1.15	+0.95
60-H-36-57	–1.11	+0.87
62-S-250	–1.42	+1.03
63-R-22	–1.71	+0.01

Using the appropriate equation from Table 11.3, estimate the temperature of formation of the sulfide ore. What are the assumptions involved in your estimate?
14. Consider the bacterial reduction of dissolved SO_4^{2-} to H_2S in a Permian marine basin in which the dissolved SO_4^{2-} had an initial δ^{34}S value of +15‰. The basin, after its formation, had no connection to the ocean but was "open" to the H_2S produced. Calculate and plot:
(a) variations in $\delta^{34}S_{SO_4}$ and the corresponding $\delta^{34}S_{H_2S}$ as the reduction progresses to completion, using the Rayleigh distillation model;
(b) corresponding variation in δ^{34}S value of the total H_2S molecules removed from the system since the beginning of fractionation, using the equation (Ohmoto and Goldhaber, 1997)

$$\delta^{34}S_{\Sigma H_2S} = (\delta^{34}S^{\text{initial}}_{SO_4} - f_{SO_4}\ \delta^{34}S^{\text{remaining}}_{SO_4})/(1 - f_{SO_4})$$

where f_{SO_4} is the atomic fraction of the SO_4^{2-} remaining in the system with respect to the original amount at any particular extent of evolution of the system. Assume constant temperature and $\alpha_{SO_4-H_2S} = 1.025$.